Thermochemical and Kinetic Analysis on the Reactions of Neopentyl and Hydroperoxy-Neopentyl Radicals with Oxygen: Part I. OH and Initial Stable HC Product Formation

Hongyan Sun and Joseph W. Bozzelli*

Department of Chemistry and Environmental Science, New Jersey Institute of Technology, Newark, New Jersey 07102

Received: May 28, 2003; In Final Form: November 13, 2003

Thermochemical properties for reactants, intermediates, products, and transition states in the neopentyl radical + O_2 reaction system are analyzed with ab initio and density functional calculations to evaluate reaction paths and kinetics for neopentyl oxidation. Enthalpies of formation ($\Delta H_f°_{298}$) are determined using isodesmic reaction analysis at the CBS-Q composite and density functional levels. The entropies ($S°_{298}$) and heat capacities $C_p(T)$ ($0 \leq T/K \leq 1500$) from vibrational, translational, and external rotational contributions are calculated using statistical mechanics based on the vibrational frequencies and structures obtained from the density functional study. Potential barriers for the internal rotations are calculated at the B3LYP/6-31G(d,p) level, and hindered rotational contributions to $S°_{298}$ and $C_p(T)$'s are calculated by using direct integration over energy levels of the internal rotation potentials. The kinetic analysis on reactions of neopentyl with O_2 is performed using enthalpies at the CBS-Q calculation level. The reaction forms a chemically activated neopentyl peroxy adduct with an energy of 38.13 kcal mol^{-1}. The energized adduct can be stabilized, dissociate back to reactants, or isomerize to the hydroperoxy-neopentyl radical. The isomer can dissociate to 3,3-dimethyloxetane + OH, to isobutene + CH_2O + OH, to methyl + 2-methyl-2-propenyl-hydroperoxide, isomerize back to the neopentyl peroxy radical, or further react with O_2. The $\Delta H_f°_{298}$ values for the neopentyl, neopentyl peroxy, and hydroperoxy-neopentyl radicals are calculated to be 10.52, −27.61, and −9.43 kcal mol^{-1}, respectively, at the CBS-Q level. Rate constants to products and stabilized adducts (isomers) of the chemically activated neopentyl peroxy are calculated as functions of pressure and temperature using quantum Rice−Ramsperger−Kassel (QRRK) analysis for $k(E)$ and a master equation analysis for the pressure falloff. An elementary reaction mechanism is constructed to model the experimental OH formation profile; the concentrations of initial products 3,3-dimethyloxetane and isobutene are also calculated by the model and compared with the experimental results. Kinetic parameters for intermediate and product-formation channels of the neopentyl + O_2 system are presented versus temperature and pressure.

Introduction

Abstraction reactions that form alkyl radicals in atmospheric and combustion reaction systems are well characterized, relative to subsequent association reactions of the radical with O_2, which form a chemically activated peroxy radical that can undergo a number of isomerization and dissociation reactions before becoming stabilized. These $R^\bullet$ + O_2 reactions are relatively complex. They involve the formation of a peroxy radical, which contains 30−40 kcal mol^{-1} of excess internal energy; this can either be lost via collision processes or used for further reaction before stabilization occurs.[1] These reactions are important rate-controlling processes in the low and intermediate temperature chemistry of hydrocarbon oxidation, especially the chemistry that occurs prior to ignition in internal combustion engines and in cool flames. The reactions of the alkyl peroxy radical intermediate are, in addition, considered essential to the prediction of negative temperature coefficient (NTC) behavior.[2] Many combustion reaction mechanisms consider the overall reaction of alkyl radicals with O_2 to form conjugate alkenes plus HO_2 to be dominant processes over the 500 to 900 K temperature range, but the details of the pathway(s) are not treated consistently, and in some cases the path is not correct. Some authors[3,4] ascribe this reaction to the abstraction of a H atom by O_2, while others[5−7] treated it by incorporating both direct molecular elimination and isomerization (hydrogen atom transfer) to a hydroperoxy-alkyl isomer that undergoes further reaction (β-scission) to products.

Two features of the neopentyl radical facilitate a simpler interpretation of experimental results relative to those of most alkyl radical oxidation systems: (a) All of the C−H bonds in the methyl groups are identical, so only one alkyl radical is involved. (b) The carbon radical site is connected to a quartenary carbon, and the formation of a C_5 conjugate alkene + HO_2 is structurally impossible by the above routes. This property of the neopentyl structure eliminates the concerted HO_2 elimination path from the peroxy adducts; only reactions involving stabilization, dissociation by reverse reaction, isomerization, and isomer decomposition are dominant here.

There are several reported experimental and modeling studies on neopentyl radical oxidation.[8−18] Hughes et al.[8,9] measured the time dependence of the OH radical from the photolysis of neopentyl iodide in a helium bath with varied concentrations of O_2 at temperatures from 660 to 750 K. An exact analytical

* To whom correspondence should be addressed. E-mail: Bozzelli@njit.edu.

10.1021/jp030667i CCC: $27.50
Published on Web 02/11/2004

SCHEME 1

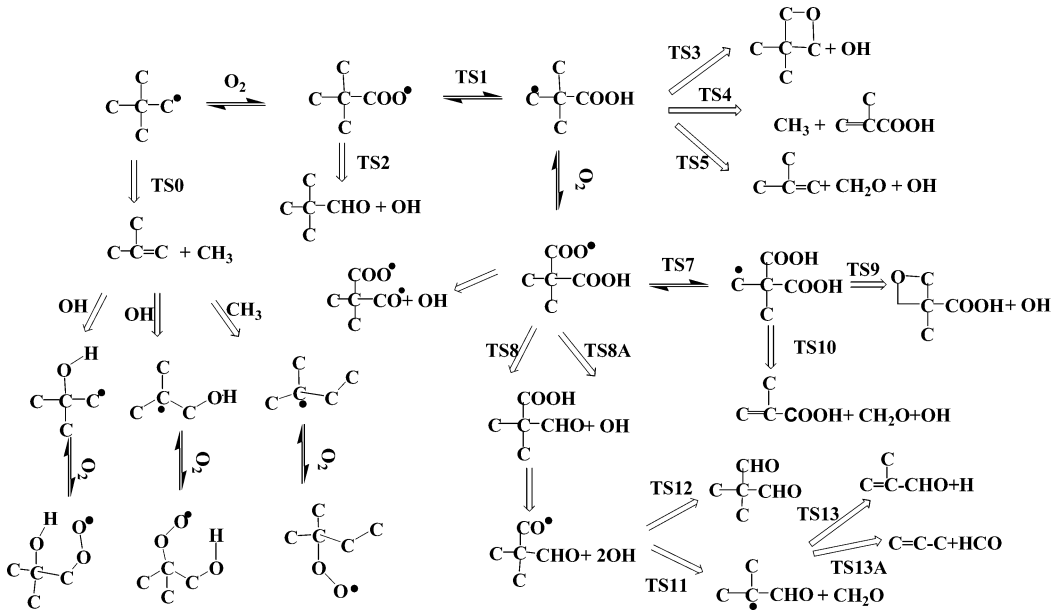

solution was postulated, incorporating neopentyl decomposition, reversible peroxy formation, and irreversible hydrogen atom transfer isomerization based on the assumption of fast subsequent decomposition via various channels to OH, which given the low species concentration present would be lost primarily by diffusion out of the photolysis zone. OH radical concentration profiles versus time were obtained by laser-induced fluorescence (LIF) and were fit to a biexponential function, which in combination with the proposed analytical solution allowed the rate coefficients for the isomerization process to be extracted and hence Arrhenius parameters to be calculated as an A factor of 1.58×10^{12} s^{-1} and an E_a value of 29 kcal mol^{-1}.

The research group of Baldwin and Walker[10,13,14] studied the reactions of the neopentyl radical in an oxidizing environment using a slow-flow reactor (reaction times up to several minutes) over the temperature range of 653−793 K at 500 Torr with product analysis by gas chromatography. The absolute concentrations of products at 753 K as a function of neopentane conversion were analyzed, and the major initial products were observed to be 3,3-dimethyloxetane, acetone, isobutene, and formaldehyde. They suggested a mechanism for the quantitative interpretation of product yields using steady state and equilibrium relationships and hence determined Arrhenius parameters for elementary reactions in their mechanism.

Bayes et al.[12] studied the rate constants of the neopentyl radical with O_2 from 266 to 374 K and at a low pressure of 3 Torr. They monitored the pseudo-first-order decay of the neopentyl radical as a function of the O_2 partial pressure using photoionization mass spectrometric detection. Their experimental results show a negative temperature dependence for the rate constant of the neopentyl radical with O_2: $k = \{2.1 \times 10^{-12}$ cm^3 molecule^{-1} s$^{-1}\}(T/300$ K$)^{-(2.1\pm0.4)}$; they suggested that this rate is essentially at its high-pressure limit (k_∞) even at 3 Torr on the basis of the comparison with studies of similar reactions. They reported that the results could be interpreted by an adiabatic channel model calculation.

Dagaut et al.[15] studied the oxidation of neopentane in a jet-stirred reactor at pressures of 1, 5, and 10 atm and at temperatures of 800 to 1230 K using probe sampling of stable species and off-line gas chromatograph analyses. They used kinetics data from the literature, THERM,[19] and kinetic estimation techniques to assemble a reaction mechanism and model the concentration profiles of the reactants, stable intermediates, and products. Their experiment and model focused on high-temperature experiments (800−1230 K), and their studies were not sensitive to reactions of peroxy radicals because the β-scission of the neopentyl radical to isobutene plus the methyl radical dominated the kinetic paths at these temperatures.

Curran et al.[18] developed a detailed kinetic model of the oxidation of neopentane and compared the experimental results at 500 Torr and 753 K by Walker et al.;[13,14] later they modified their mechanism in conjunction with new data from high-pressure flow reactor experiments.[17] They estimated thermochemical and kinetic parameters using THERM[19] and other techniques to model stable end-product profiles without transition-state or falloff analysis.

Taatjes et al.[7] recently measured the time-resolved production of OH and HO_2 for the pulsed-photolytic Cl-initiated oxidation of neopentane between 573 and 750 K. They reported that the isomerization of the initially formed RO_2 radical to form the QOOH species is very rapid and that direct pathways of OH production from chemical activation reactions $R^\bullet + O_2$ are essential to the correct modeling of oxidation reactions. They also proposed a kinetic mechanism for modeling their experimental OH and HO_2 profiles versus time and temperature. The peroxy reactions were based on their previous time-dependent master equation calculation of analogous processes in the reaction of *n*-propyl with O_2.

Thermochemical and kinetic parameters in our theoretical model are based on ab initio and density functional calculations, and the reaction mechanism for the neopentyl radical + O_2 system is outlined in Scheme 1.

The treatment of the energized complex reactions in our mechanism includes an analysis of the decomposition back to reactants and the intramolecular transfer of hydrogen atoms to form a hydroperoxy alkyl radical, which can dissociate to products before stabilization. Further isomerizations and dissociations of the stabilized neopentyl peroxy radical and the hydroperoxide alkyl isomer are also included along with a second O_2 addition to the hydroperoxy-neopentyl radical. Several other important reaction paths, as illustrated above, are also included in the elementary reaction mechanism.

Thermochemical properties of reactants, intermediates, products, and transition states for the elementary reactions are

calculated by ab initio and density functional calculations with an analysis of internal rotation barriers at the DFT level. High-pressure-limit rate constants are calculated by canonical transition-state theory or evaluated from the literature. Quantum RRK theory[20−23] is used for the analysis of $k(E)$, and a master equation[6] is used for analysis of the falloff in kinetic analysis of the chemical activation and unimolecular dissociation reaction systems. The rate constants are incorporated into an elementary reaction mechanism and are shown to model Hughes et al.'s[9] experimental OH profile well. Concentrations of the initial stable product profiles observed by Walker et al.,[13,14] reported as a function of neopentane conversion, are also calculated by our mechanism. The present kinetic scheme is also used as a starting reaction mechanism to model the HO_2 formation at the experimental conditions of Taatjes et al.[7] in a follow-up paper to this study. HO_2 is a secondary product, and further oxidation reactions of the initial hydrocarbon and oxyhydrocarbon intermediates need to be included to model it.

Calculation Method

Computational Details. The geometries of reactants, important intermediates, transition states, and products in the neopentyl + O_2 reaction system are preoptimized using PM3 MOPAC[24] calculations, followed by optimizations and frequency calculations at the B3LYP/6-31G(d,p) level using the Gaussian 98 program.[25] The optimized structure parameters are then used to obtain total electronic energies at the B3LYP/6-311++G(3df,2p) and CBS-Q single-point levels of calculation. The potential energies for the neopentyl + O_2 system are calculated at the CBS-Q level. For the secondary reaction system, the addition of $^3O_2$ to the hydroperoxy neopentyl radical, the potential energies are calculated at the B3LYP/6-311++G(3df,2p) level because of the relatively large molecule size. For iodine-containing species, the effective core-potential basis sets, modified diffuse sp functions, and d polarization function are employed.[26,27] Rotational barriers for the internal rotational potentials are calculated at the B3LYP/6-31G(d,p) level.

Thermochemical Properties. Contributions from vibrational, translational, external rotational, and electronic degeneracy to entropies and heat capacities are calculated by statistical mechanics based on the vibrational frequencies and moments of inertia from the DFT optimized structures. The torsion frequencies are identified by viewing bond motions using the GaussView 98 program;[28] these torsion frequencies are omitted in calculations of $S°_{298}$ and $C_p(T)$, and their contributions are replaced with values from the analysis of the internal rotations. Contributions from hindered rotors to $S°_{298}$ and $C_p(T)$ values are determined by solving the Schrödinger equation with free rotor wave functions, and the partition coefficients are obtained by direct integration over the energy levels of the intramolecular rotational potential curves that are represented by a truncated Fourier series expansion. The $\Delta H_f°_{298}$ values for reactants, intermediates, and products are calculated using total energies from ab initio and DFT calculations and isodesmic reactions with group balance when possible. Transition-state (TS) geometries are identified by the existence of only one imaginary frequency in the normal mode coordinate analysis, an evaluation of the TS geometry, and the reaction coordinate's vibrational motion. The $\Delta H_f°_{298}$ values of transition-state structures are calculated from the $\Delta H_f°_{298}$ values of the stable radical adducts from working isodesmic reaction analysis plus the difference in the total energies between the radical adducts and the transition states.

Kinetic Analysis. Unimolecular dissociation and isomerization reactions of the chemically activated and stabilized adducts resulting from addition or combination reactions are analyzed by first constructing potential energy diagrams for the reaction system. DFT and ab initio calculations are used to calculate transition-state structures and activation energies for isomerization, β-scission, and dissociation reactions. The enthalpies and entropies are treated with conventional transition-state theory to calculate Arrhenius preexponential factors and energies of activation that result in high-pressure-limit rate constants (k_∞) as functions of temperature. Nonlinear Arrhenius effects resulting from changes in the thermochemical properties of the respective transition state relative to those of its adduct with temperature are incorporated using a two-parameter Arrhenius preexponential factor (A, n) in AT^n. High-pressure-limit preexponential factors for association reactions are obtained from the literature. Equilibrium constants $K_{eq}(T)$ are calculated from thermodynamic properties of reactants and products as a function of temperature. Reverse rate constants are calculated from the principle of microscopic reversibility. Branching ratios of the energized adduct to stabilization and product channels are calculated using multifrequency quantum Rice−Rampsperger−Kassel (QRRK) analysis for $k(E)$[19,29] with the steady-state assumption for the energized adduct(s) in combination with a master equation analysis[6,30] for pressure falloff.

The QRRK calculation evaluates energy-dependent rate constants, $k(E)$, of the energized adduct to each channel for the bimolecular chemical activation reaction and includes equilibrium in isomerization reactions. The QRRK analysis described by Chang et al.[23] and Sheng et al.[6] is shown to yield reasonable results and provides a framework by which the effects of temperature and pressure can be evaluated in these complex reaction systems. The QRRK code utilizes a reduced set of three vibrational frequencies and their associated degeneracies that accurately reproduce the adduct heat capacity and include one external rotation in the calculation of accurate ratios of the density of states to the partition coefficient, $\rho(E)/Q$.[31]

Evaluations of the steady-state QRRK chemical activation analysis we utilize indicate that it is valid for reaction times on the order of microseconds; an analysis for longer times of reaction may require the use of CHEMKIN analysis in order to include reactions of the stabilized adducts depending on temperature, pressure, and rate constants.

A 0.5-kcal energy grain is used to obtain rate constants as a function of temperature and pressure for chemical activation and dissociation reactions. $(\Delta E)°_{down}$ values of 570, 621, and 1000 cal mol^{-1} are used in the master equation analysis with He, H_2, and O_2 as the third body, respectively. Lennard-Jones parameters, σ (Å), and ϵ/κ (K) are obtained from tabulations[32] and from an estimation method based on molar volumes and compressibility.

Results and Discussion

1. Geometries of Reactants, Intermediate Radicals, and Transition States. The geometry optimizations for the reactants, transition states, adducts, and products in the neopentyl oxidation system are performed at the B3LYP/6-31G(d,p) level, and the effective core-potential basis sets, modified diffuse sp functions, and d polarization function[27] are used for iodine-containing species. The optimized structural parameters for 33 species including transition-state structures are listed in Supporting Information Table S1. The corresponding unscaled vibrational frequencies and moments of inertia are listed in Table S2. Several important species in this system are defined as $C_3CC^•$

(neopentyl radical), $C_3CCOO^•$ (neopentyl peroxy radical), $C_3^•CCOOH$ (hydroperoxy-neopentyl radical), $C_2CYCCOC$ (3,3-dimethyloxetane), $C_2C(OOH)COO^•$ (hydroperoxy-neopentyl-peroxy radical), $C_2^•C(COOH)_2$ (dihydroperoxide-neopentyl radical), C(COOH)CYCCOC (3-methyl,3-hydroperoxideoxetane), C═C(C)COOH (isobutenyl hydroperoxide), $C_2C(COOH)CHO$ (2-methyl isopropanal-2-methylhydroperoxide), $C_2C(CHO)-CH_2O^•$ (2-methyl isopropanal-2-methyoxy radical), and C_3CCI (neopentyliodide). The transition states of important reactions in this oxidation system are identified as follows:

Alkyl Peroxy Radical Isomerization.

$$C_3CCOO^• \rightarrow TS1 \rightarrow C_3^•CCOOH$$

$$C_2C(OOH)COO^• \rightarrow TS7 \rightarrow C_2^•C(COOH)_2$$

These reactions represent the intramolecular, endothermic transfer of a H atom from a primary methyl carbon atom to the peroxy oxygen radical site via a six-membered-ring transition state including the H atom. The cleaving C—H bond stretches to 1.40 Å from 1.09 Å, and the forming O—H bond length is 1.14 Å, which is longer than that of a normal O—H bond, 0.978 Å.

Epoxide Formation.

$$C_3^•CCOOH \rightarrow TS3 \rightarrow C_2CYCCOC + OH$$

$$C_2^•C(COOH)_2 \rightarrow TS9 \rightarrow C(COOH)CYCCOC + OH$$

In this type of reaction, the carbon radical in the $-CH_2^•$ group attacks the peroxy oxygen to form a four-membered-ring transition state while the weak RO—OH bond is breaking. The length of the cleaving O—O bond is 1.68 Å, and the length of the forming C—O bond is 1.99 Å. This reaction is responsible for a major fraction of the OH formation.

β-Scission of Alkyl Radicals.

$$C_3CC^• \rightarrow TS0 \rightarrow C_2C{=}C + CH_3$$

$$C_3^•CCOOH \rightarrow TS4 \rightarrow C_2C{=}C + CH_2O + OH$$

$$C_3^•CCOOH \rightarrow TS5 \rightarrow C{=}C(C)COOH + CH_3$$

$$C_2^•C(COOH)_2 \rightarrow TS10 \rightarrow C{=}C(C)COOH + CH_2O + OH$$

These reactions involve the cleavage of an alkyl or oxyalkyl group moving perpendicular from a near-planar isobutenyl structure with the simultaneous formation of a π bond (olefin here) on the adjacent carbon. For methyl group dissociation, the C—C bond length stretches from 1.58 to 2.31 Å, and the length of the forming C═C bond is 1.37 Å in the TS0 and TS5 structures.

At temperatures above 1200 °C, the unimolecular dissociation of the neopentyl radical via TS0 is the primary reaction relative to the reaction with O_2.

For the $CH_2O + OH$ elimination from $C_3^•CCOOH$ in TS4, the C—O bond length in the leaving group is decreased slightly from 1.425 to 1.366 Å, and O—O bond length is slightly increased in length from 1.457 to 1.470 Å.

In the structure of TS10, the C—O bond length (1.31 Å) is shorter than that of TS4, and the O—O bond length (1.78 Å) is longer than that of TS4 because of the interaction of the hydroperoxy H and O atoms between the two −COOH groups (Table S1).

OH Elimination from the Alkyl Peroxy Group.

$$C_3CCOO^• \rightarrow TS2 \rightarrow C_3CCHO + OH$$

$$C_2C(OOH)COO^• \rightarrow TS8A \rightarrow C_2C(COOH)CHO + OH$$

In this reaction group, the peroxy oxygen radical attacks the H atom in the nearest carbon via a four-membered-ring transition state. The reaction path passes through a transient intermediate $R-C^•OOH$, where the carbon radical forms a π (carbonyl) bond with the oxygen (gaining ca. 80 kcal mol^{-1}) and cleaves the weak O—OH bond (requiring only ca. 45 kcal mol^{-1}). The C—O (forming), O—O (cleaving), and O—H bond lengths are 1.39, 1.50, and 1.27 Å, respectively. The changes in these bond lengths between the reactant and TS suggest that the transition state reacts through the $R-C^•OOH$ structure to the intermediate R—CH(═O) + OH.

2. Thermochemical Properties $\Delta H_f^\circ_{298}$, S°_{298}, and C_p(300) to C_p(1500). *Enthalpies of Formation.* The enthalpies of formation for reactants, intermediate adducts, and products in the neopentyl oxidation system are calculated by isodesmic reaction analysis or taken from available literature. Table 1 lists the calculated reaction enthalpies and $\Delta H_f^\circ_{298}$ values for the species in the $C_3CC^• + O_2$ system at three calculation levels. The calculated $\Delta H_f^\circ_{298}$ values from the DFT calculations show good agreement with the higher-level ab initio calculations, indicating that the errors in the computations for different molecules are canceled to a significant extent, ca. ± 2 kcal mol^{-1}, by the working reactions. The agreement between the calculation levels and with the literature data suggests reasonable accuracy for the absolute enthalpy values. The average $\Delta H_f^\circ_{298}$ values from the higher-level CBS-Q calculations are selected to construct our kinetic model.

Enthalpies for transition states are calculated by the use of two methods. The first method is straightforward using the $\Delta H_f^\circ_{298}$ values of the stable radical adducts from the working reaction analysis plus the differences with calculated total energy between the radical adduct and the corresponding transition state structure. The second method takes an average of (i) the calculated energy difference between the TST structure and the reactant and (ii) the difference between the TST and the products plus the enthalpy of reaction (ΔH°_{rxn}). The ΔH°_{rxn} values are calculated from the $\Delta H_f^\circ_{298}$ values of the reactant and product, which are determined on an absolute basis by the working reaction analysis. Enthalpies of formation for six transition states in the $C_3CC^• + O_2$ system determined by these two methods at the three different levels are listed in Table 2. It can be seen that the reaction enthalpies calculated from the forward reaction (method 1) show good agreement with the average values (method 2) for all six reactions at the CBS-Q level. The reaction enthalpies from DFT calculations show good agreement only with the values from the CBS-Q level for the reactions with tight transition states (ring formation). Enthalpies of formation for transition states calculated from the first method at the CBS-Q level are used for our kinetic model.

The $\Delta H_f^\circ_{298}$ of the neopentyl radical is calculated to be 10.52 kcal mol^{-1} at the CBS-Q level, which gives the C_3CC—H bond dissociation energy of 102.76 kcal mol^{-1} based on the published $\Delta H_f^\circ_{298}$ value for neopentane (−40.14 ± 0.15 kcal mol^{-1}).[33] The above enthalpy value shows good agreement with the value of 10.36 kcal mol^{-1} reported recently by Sumathi el al. at the CBS-Q calculation level.[34] Holmes el al.[35] measured the heats of formation of alkyl radicals by monoenergetic electron impact,

TABLE 1: Calculated $\Delta H_f^\circ{}_{298}$ Values for Species in the $C_3CC^\bullet + O_2$ System[a]

	B3LYP/6-31G(d,p)		B3LYP/6-311++G(3df,2p)		CBS-Q//B3LYP/6-31G(d,p)	
reaction series	ΔH°_{rxn}	$\Delta H_f^\circ{}_{298}$	ΔH°_{rxn}	$\Delta H_f^\circ{}_{298}$	ΔH°_{rxn}	$\Delta H_f^\circ{}_{298}$
1. $C_3CCOOH + COH \rightarrow C_3COH + CCOOH$	−10.29	−56.06	−10.10	−56.25	−7.65	−58.70
2. $C_3CCOOH + CCOH \rightarrow C_3COH + CCCOOH$	−6.12	−57.25	−6.33	−57.04	−4.83	−58.54
3. $C_3CCOOH + CCOH \rightarrow C_3CCOH + CCOOH$	−1.10	−58.54	−2.18	−57.46	−1.06	−58.58
average $\Delta H_f^\circ{}_{298}$ at CBS-Q level:						**−58.60**
1. $C_3CCOO^\bullet + CH_3OOH \rightarrow C_3CCOOH + CH_3OO^\bullet$	0.52	−26.08	0.55	−26.10	2.08	−27.63
2. $C_3CCOO^\bullet + CCOOH \rightarrow C_3CCOOH + CCOO^\bullet$	0.81	−26.51	0.84	−26.54	1.83	−27.53
3. $C_3CCOO^\bullet + C_2COOH \rightarrow C_3CCOOH + C_2COO^\bullet$	0.24	−27.05	0.06	−26.88	0.84	−27.65
average $\Delta H_f^\circ{}_{298}$ at CBS-Q level:						**−27.61**
1. $C_3^\bullet CCOOH + C_2H_6 \rightarrow C_3CCOOH + C_2H_5$	−0.51	−9.05	−0.65	−8.91	−0.12	−9.45
2. $C_3^\bullet CCOOH + CCOOH \rightarrow C_3CCOOH + C^\bullet COOH$	−3.80	−7.42	−3.62	−7.59	−1.80	−9.41
3. $C_3^\bullet CCOOH + CCOH \rightarrow C_3CCOOH + C^\bullet COH$	1.16	−9.34	0.62	−8.81	1.26	−9.44
average $\Delta H_f^\circ{}_{298}$ at CBS-Q level:						**−9.43**
1. $C_3CC^\bullet + CH_4 \rightarrow C_3CC + CH_3$	3.73	8.80	3.53	9.00	2.01	10.52
2. $C_3CC^\bullet + C_2H_6 \rightarrow C_3CC + C_2H_5$	−1.03	9.89	−1.17	10.03	−1.65	10.51
average $\Delta H_f^\circ{}_{298}$ at CBS-Q level:						**−10.52**
1. $C_3CCHO + CH_4 \rightarrow C_3CC + CH_2O$	11.76	−59.99	11.22	−59.45	10.30	−58.53
2. $C_3CCHO + C_2H_6 \rightarrow C_3CC + CH_3CHO$	0.22	−59.86	−0.52	−59.12	−0.69	−58.95
average $\Delta H_f^\circ{}_{298}$ at CBS-Q level:						**−58.74**
1. $C{=}C(C)COOH + CH_4 \rightarrow C{=}CCOOH + C_2H_6$	6.21	−19.93	5.79	−19.50	8.65	−22.36
2. $C{=}C(C)COOH + CH_3OH \rightarrow C{=}CCOOH + CCOH$	0.74	−20.16	0.79	−20.21	2.93	−22.34
average $\Delta H_f^\circ{}_{298}$ at CBS-Q level:						**−22.35**
1. $CCC^\bullet(C)COOH \rightarrow C_3^\bullet CCOOH$	6.36	−15.79	6.07	−15.50	0.98	−10.42
$\Delta H_f^\circ{}_{298}$ at CBS-Q level:						**−10.42**

[a] kcal mol^{-1}.

TABLE 2: Reaction Enthalpies in the Reactions of Neopentyl + O_2[a]

	B3LYP /6-31G(d,p)	B3LYP /6-311++G(3df,2p)	CBS-Q//B3LYP /6-31G(d,p)	B3LYP /6-31G(d,p)	B3LYP /6-311++G(3df,2p)	CBS-Q//B3LYP /6-31G(d,p)
	$E_{a,\ forward}$[b]	$E_{a,\ forward}$[b]	$E_{a,\ forward}$[b]	$E_{a,\ average}$[c]	$E_{a,\ average}$[c]	$E_{a,\ average}$[c]
TS1	24.00	23.42	23.82	21.65	22.79	23.90
TS2	42.54	42.06	41.61	40.36	43.59	42.21
TS3	14.71	14.14	15.51	14.88	15.74	16.12
TS4	29.97	27.81	25.39	31.82	31.69	25.31
TS5	24.19	22.49	26.52	29.58	32.00	26.36
TS6	54.35	53.23	56.34	57.25	55.98	56.55

[a] kcal mol^{-1}. [b] Reaction enthalpies are calculated from forward reaction. [c] Reaction enthalpies are calculated from the average enthalpy values of the forward, reverse, and ΔH°_{rxn}. $E_{a,average} = {}^1/_2(E_{a,\ forward} + E_{a,\ reverse} + \Delta H^\circ_{rxn})$.

TABLE 3: Comparison of Calculated $\Delta H_f^\circ{}_{298}$ at CBS-Q with Experimental Values

	enthalpies of formation ($\Delta H_f^\circ{}_{298}$) in kcal/mol				
species	CBS-Q	literature	species	CBS-Q	literature
CH_3CH_2OOH	−39.9 ± 1.5	−39.7 ± 0.3[38]	$CH_3CH_2O^\bullet$	−3.90 ± 1.27	−3.7 ± 0.8[39]
$CH_3CH_2OO^\bullet$	−6.7 ± 2.3	−6.8 ± 2.3[40]	$CH_3C^\bullet HOH$	−13.34 ±0.84	−14.5 ± 3[41]
$C^\bullet H_2CH_2OOH$	11.2 ± 2.1	10.96 ±1.06[38]	$CH_2^\bullet CH_2OH$	5.70 ± 0.85	−5.9[42]
$CH_3C^\bullet(=O)$	−3.08 ±0.38	−2.90 ± 0.70[43]	$(CH_3)_2CHOH$	−69.19 ± 0.31	−69.15[44]
$CH_2^\bullet OH$	−3.97±1.11	−3.97 ± 0.22[45,46]	$(CH_3)_2CHO^\bullet$	−11.85 ± 0.08	−11.0 ± 1.2[47]

and they reported that their values agree with results from equivalent measurements using ESR spectroscopy. They reported a $\Delta H_f^\circ{}_{298}$ value of 10.1 kcal mol^{-1} for the neopentyl radical.

The $\Delta H_f^\circ{}_{298}$ of neopentyl peroxy is calculated to be −27.61 kcal mol^{-1} at the CBS-Q level; Curran et al.[17] estimated it to be −26.80 kcal mol^{-1} by group additivity using THERM.[19] The reaction enthalpies of alkyl radicals + O_2 are reported by Knyazev[36] to be 32.74, 35.47, 37.14, and 36.52 kcal mol^{-1} for CH_3, C_2H_5, *i*-C_3H_7, and *t*-C_4H_9, respectively, which are obtained from the third-law treatment of the temperature dependencies of the equilibrium constants $K_p(T)$. Clifford et al.[37] reviewed the thermochemistry of alkyl peroxy radicals and gives the reaction enthalpy of *tert*-butyl + O_2 as −37 ± 2 kcal mol^{-1}. The well depth for $C_3CC^\bullet + O_2$ is calculated to be 38.13 kcal mol^{-1} in this work.

The $\Delta H_f^\circ{}_{298}$ values of hydrocarbons, substituted hydrocarbons, and corresponding radicals have been investigated in our previous studies, which show that the CBS-Q enthalpy values based on B3LYP/6-31G(d,p) optimized geometries are in agreement with accepted literature values. The CBS-Q enthalpies are more consistent than those from QCISD(T)/6-31G(d,p) single-point calculations when the values for one species are compared through a series of different working reactions. A comparison of $\Delta H_f^\circ{}_{298}$ values from CBS-Q calculations with experimental data or accepted literature data on several oxygenated hydrocarbons is listed in Table 3.

Internal Rotation Analysis. The calculated internal rotation potentials on the C—C bonds of the neopentyl peroxy radical and the hydroperoxide neopentyl radical are shown in Figure 1, where the normal 3-fold barrier for rotation on the CH_3—C bonds is illustrated. The barriers for methyl rotors are near 3.3, and the C_3C—$COO^\bullet$ barriers are near 5 kcal mol^{-1}. Figure 2 shows the rotation potentials on the C—OOH, C—$OO^\bullet$, and CO—OH bonds for the above two species, which have relatively high barriers of 4 to 7.5 kcal mol^{-1}. The 6 and 7 kcal mol^{-1}

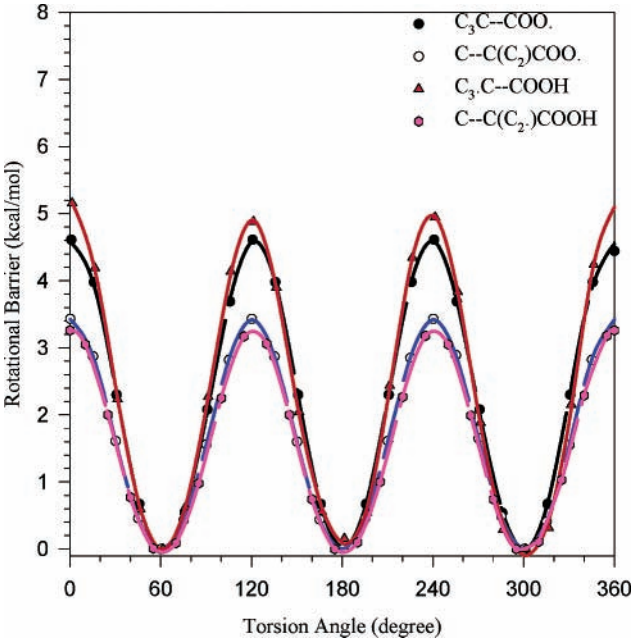

Figure 1. Torsional potentials on the C—C bond of the neopentyl peroxy radical and hydroperoxy-neopentyl radical calculated at the B3LYP/6-31G(d,p) level.

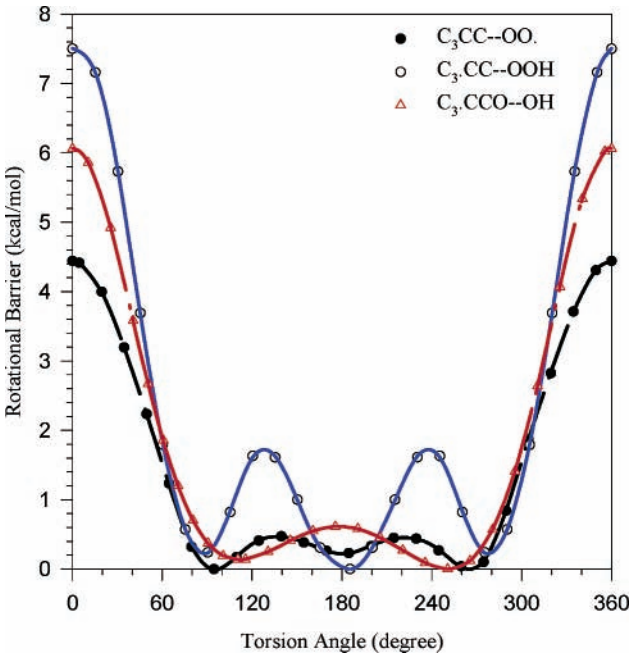

Figure 2. Torsional potentials on the C—O and O—O bonds of the neopentyl peroxy radical and the hydroperoxy-neopentyl radical calculated at the B3LYP/6-31G(d,p) level.

barrier heights are typical of published data on these CO—OH and C—OOH bonds.[48,49]

The torsional potential on the CH_2•—C(C_2)COOH bond in Figure 3 shows a very low, 6-fold barrier, where only two wells have depths greater than 0.3 kcal mol^{-1}. This CH_2•—C(C_2)-COOH rotor is nearly a free rotor. Figure 3 shows both UB3LYP/6-31G(d,p) and UMP2/6-31G(d,p) calculations, where the barriers are low and of similar symmetry but the energies are somewhat different. We choose the potential curve from the UB3LYP/6-31G(d,p) level to calculate the contribution from the CH_2•—C(C_2)COOH internal rotor to $S°_{298}$ and $C_p(T)$ values for consistency. Table 4 illustrates the values from vibrational, translational, external rotational contributions, and also each

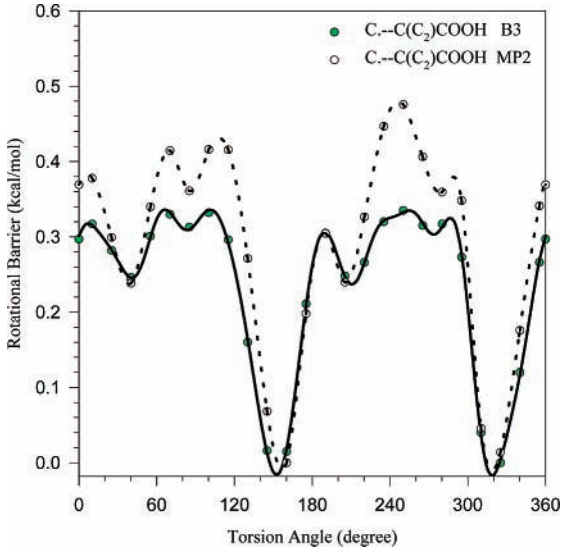

Figure 3. Torsional potentials on the C•—C bond of the hydroperoxy-neopentyl radical calculated at the B3LYP/6-31G(d,p) and MP2/6-31G(d,p) levels.

hindered internal rotational contribution to $S°_{298}$ and $C_p(T)$ values for C_3CCOO• and C_3•CCOOH. Table 5 lists the thermochemical properties of important reactants, transition states, adducts, and products calculated in this work.

3. Chemical Activation Reaction Analysis. *3.1. C_3CC•+ O_2.* A potential energy diagram for the C_3CC• + O_2 reaction system calculated at the CBS-Q level is shown in Figure 4. The neopentyl radical ($\Delta H_f°_{298}$ = 10.52 kcal mol^{-1}) reacts with O_2 to form a C_3CCOO• radical with a 38.13 kcal mol^{-1} well depth. Reaction channels for the energized adduct C_3CCOO•* include dissociation back to reactants, stabilization to C_3CCOO•, isomerization by hydrogen transfer to the peroxy radical site via TS1 (E_a = 23.82 kcal mol^{-1}) to form a C_3•CCOOH isomer ($\Delta H_f°_{298}$ = −9.43 kcal mol^{-1}), and dissociation to products (C_3CCHO + OH) via TS2 (E_a = 41.61 kcal mol^{-1}). The barrier for C_3CCOO• isomerization to C_3•CCOOH is calculated to be 23.82 kcal mol^{-1}; therefore, the chemically activated C_3CCOO•* adduct has sufficient energy for this isomerization to occur before it is stabilized or reacts back to reactants (reverse). Because the energy of TS3 is ca. 4 kcal mol^{-1} lower than that of the entrance channel, the chemically activated C_3CCOO•* adduct can isomerize and dissociate to 3,3-dimethyloxetane + OH directly.

The energized C_3•CCOOH isomer undergoes unimolecular reaction through several forward channels that are important to products or revert back to the peroxy isomer. Forward reactions are dissociation to 3,3-dimethyloxetane + OH via TS3 (E_a = 15.50 kcal mol^{-1}), β-scission to C_2C═C + CH_2O + OH via TS4 (E_a = 25.38 kcal mol^{-1}), and another β-scission (elimination) to C═C(C)COOH + CH_3 via TS5 (E_a = 26.52 kcal mol^{-1}). The C_3•CCOOH isomer can also undergo a very interesting isomerization via TS6 (E_a = 56.34 kcal mol^{-1}) shifting a methyl group onto the $-CH_2$• radical site forming a tertiary radical, but the high barrier and tight transition state make this channel unimportant. The dominant channel of this hydroperoxy-neopentyl isomer is the reverse reaction back to the peroxy isomer, with a barrier of only 5.64 kcal mol^{-1}.

The stabilized C_3•CCOOH isomer's dissociation to 3,3-dimethyloxetane + OH via TS3 is very important to the formation of OH and the initial 3,3-dimethyloxetane product. The barrier for this channel is calculated to be 15.50 kcal mol^{-1} at the CBS-Q level, and it shows good agreement with Benson's

TABLE 4: Thermodynamic Properties of $C_3CCOO^\bullet$ and $C_3{}^\bullet CCOOH$[a]

species		$\Delta H_f°_{298}$[b]	$S°_{298}$[c]	C_p300[c]	C_p400	C_p500	C_p600	C_p800	C_p1000	C_p1500
$C_3CCOO^\bullet$	TVR[d]		69.17	24.39	32.62	40.25	46.84	57.22	64.90	76.80
(81)[f]	C−O[e]		6.82	1.45	1.47	1.50	1.50	1.46	1.38	1.15
	C(neo)−COO[e]		6.63	2.19	2.28	2.29	2.22	1.95	1.65	1.06
	C−C(neo)[e]		4.30	2.07	2.14	2.07	1.95	1.70	1.52	1.27
	C−C(neo)[e]		4.30	2.07	2.14	2.07	1.95	1.70	1.52	1.27
	C−C(neo)[e]		4.30	2.07	2.14	2.07	1.95	1.70	1.52	1.27
$C_3CCOO^\bullet$		−27.61	95.53	34.25	42.79	50.24	56.40	65.74	72.49	82.81
$C_3{}^\bullet CCOOH$	TVR[d]		75.11	25.57	33.53	40.75	46.89	56.54	63.71	75.03
(9)[f]	O−O[e]		3.59	1.39	1.41	1.44	1.46	1.47	1.45	1.34
	C−O[e]		6.68	2.05	1.84	1.71	1.63	1.54	1.47	1.23
	C(neo)−COOH[e]		6.37	2.10	2.16	2.19	2.16	1.98	1.75	1.22
	C−C(neo)[e]		4.34	2.08	2.13	2.05	1.93	1.68	1.50	1.26
	C−C(neo)[e]		4.34	2.08	2.13	2.05	1.93	1.68	1.50	1.26
	C−C(neo)[e]		5.15	1.06	1.03	1.02	1.01	1.00	1.00	1.00
$C_3{}^\bullet CCOOH$		−9.43	105.58	36.33	44.23	51.20	57.00	65.90	72.37	82.33

[a] Thermodynamic properties are referred to the standard state of an ideal gas at 1 atm. [b] kcal mol^{-1}. [c] cal mol^{-1} K^{-1}. [d] Sum of contributions from translations, vibrations, and external rotations. [e] Contribution from internal rotations. [f] Symmetry number.

TABLE 5: Ideal Gas-Phase Thermodynamic Properties[a]

species	$\Delta H_f°_{298}$[b]	$S°_{298}$[c]	C_p300[c]	C_p400	C_p500	C_p600	C_p800	C_p1000	C_p1500
TS0	40.26	82.76	30.15	37.27	43.34	48.39	56.38	62.50	72.50
TS1	−3.79	86.14	32.97	42.15	50.04	56.54	66.39	73.48	84.33
TS2	14.00	91.47	34.65	43.25	50.66	56.75	65.98	72.63	82.73
TS3	6.07	99.54	36.69	44.85	51.89	57.72	66.64	73.16	83.25
TS4	15.95	102.77	36.95	44.78	51.52	57.09	65.60	71.82	81.50
TS5	17.09	102.36	37.28	45.17	51.96	57.58	66.17	72.48	82.28
TS6	46.91	102.39	35.20	43.36	50.52	56.49	65.63	72.27	82.38
TS7	−19.41	105.79	40.08	50.14	58.82	65.90	76.36	83.63	94.23
TS8	19.99	100.61	40.36	50.36	58.92	65.92	76.38	83.78	94.93
TS8A	−1.61	111.40	41.56	51.02	59.21	65.93	75.95	82.98	93.36
TS9	−9.42	112.81	42.59	51.94	59.95	66.46	76.16	83.04	93.48
TS10	−10.21	115.74	44.58	53.40	60.98	67.21	76.60	83.34	93.66
$C_3CC^\bullet$	10.52	81.78	29.19	36.48	42.80	48.07	56.32	62.56	72.65
C_3CCOOH	−58.60	97.52	36.47	45.10	52.70	59.05	68.78	75.87	86.80
$C_3CCOO^\bullet$	−27.61	95.53	34.25	42.79	50.24	56.40	65.74	72.49	82.81
$C_3{}^\bullet CCOOH$	−9.43	105.58	36.33	44.23	51.20	57.00	65.90	72.37	82.33
$CCC^\bullet(C)COOH$	−10.42	105.33	34.15	42.22	49.50	55.64	65.07	71.89	82.22
C_3CCHO	−58.74	84.46	30.19	37.07	43.21	48.47	56.84	63.17	73.19
$C_2CYCCOC$	−35.43	81.19	27.04	34.90	42.01	48.02	57.35	64.21	74.77
$C_2CYCCOC^\bullet$	10.92[d]	76.30	23.71	31.05	37.51	42.88	51.13	57.16	66.48
C═C(C)COOH	−22.35	93.34	30.43	35.88	40.71	44.81	51.26	56.11	63.71
$C_2C(COOH)COO^\bullet$	−42.39	118.81	42.07	51.27	59.34	65.95	75.77	82.61	92.62
$C_2{}^\bullet C(COOH)_2$	−25.14	125.55	43.47	52.28	60.03	66.42	75.91	82.54	92.23
$C_2C(COOH)CHO$	−76.83	108.44	37.16	44.89	51.85	57.73	66.77	73.29	83.07
$C(COOH)CYCCOC$	−52.37	101.84	34.02	42.89	50.85	57.48	67.44	74.43	84.69
$C_2C(CH_2O^\bullet)COO^\bullet$	−8.25	107.37	37.55	46.35	53.88	59.98	69.01	75.34	84.80
$C_2C(CHO)CH_2O^\bullet$	−40.63	96.23	32.75	39.98	46.29	51.56	59.65	65.51	74.40
$C_2C(CHO)_2$	−75.03	93.95	30.90	37.05	42.59	47.37	54.96	60.61	69.36
$C_2C^\bullet CHO$	−19.16	79.12	22.01	26.89	31.59	35.74	42.41	47.37	55.03
C_3CCI	−15.35	86.23	32.13	40.40	47.51	53.35	62.24	68.73	78.89
$C_3{}^\bullet CCI$	36.07	93.63	32.07	39.81	46.33	51.61	59.52	65.29	74.34
CH_2I	55.00[e]	66.30	11.58	12.55	13.30	13.86	14.58	15.00	15.47
$IO^\bullet$	27.70[f]	57.43	7.89	8.24	8.45	8.59	8.73	8.80	8.88

[a] Thermodynamic properties are referred to the standard state of an ideal gas of a pure enantiometer at 1 atm. [b] kcal mol^{-1}. [c] cal mol^{-1} K^{-1}. [d] Based on the parent- and bond-energy calculations. [e] Furuyama, S.; Golden, D. M.; Benson, S. W. *Int. J. Chem. Kinet.* **1969**, 1, 283. [f] Bedjanian, Y.; Bras, G. L.; Poulet, G. *J. Phys. Chem.* **1997**, *101*, 4088.

estimate of 15.06 kcal mol^{-1} for the decomposition of alkylhydroperoxide radicals into oxetanes and also Curran's estimate[18] of 15.25 kcal mol^{-1}. Wijaya et al.[50] calculated this barrier height to be 19.5 and 21.0 kcal mol^{-1} at the CBS-QB3 and BH&HLYP/6-311G** levels. DeSain el al.[7] calculated this barrier to be 15.08 kcal mol^{-1} at the B3LYP/6-31G* level and adjusted it to19.98 kcal mol^{-1} by the difference between the B3LYP/6-31G* and the QCISD(T)/6-311++G(3df,2pd) energies of analogous *n*-propyl + O_2 stationary points. In this work, this barrier is calculated to be 18.83 kcal mol^{-1} at the CBS-QB3 level, but in the CBS procedure for the extrapolation of energies, we observed a 2.91 kcal mol^{-1} overstabilization of $\Delta\Delta E$(Emp) that contributes to the CBS-QB3 barrier height; this quantity appears to be 0.36 kcal mol^{-1} in the CBS-Q calculation. The barrier height, 15.50 kcal mol^{-1}, is therefore more reliable for use in the kinetic model. However, the spin contamination in both of our CBS calculations for TS3 is high; the expectation values of $\langle S^2 \rangle$ are 1.23 and 1.25 in the CBS-Q and CBS-QB3 calculations, respectively. The density functional calculations do not show the high spin contamination (the expectation values of $<S^2>$ are around 0.79) and show forward direction values of 14.71 to 14.14 kcal mol^{-1}, which support the value we use.

3,3-Dimethyloxetane is an important primary product; it can undergo an abstraction reaction to lose a secondary H atom

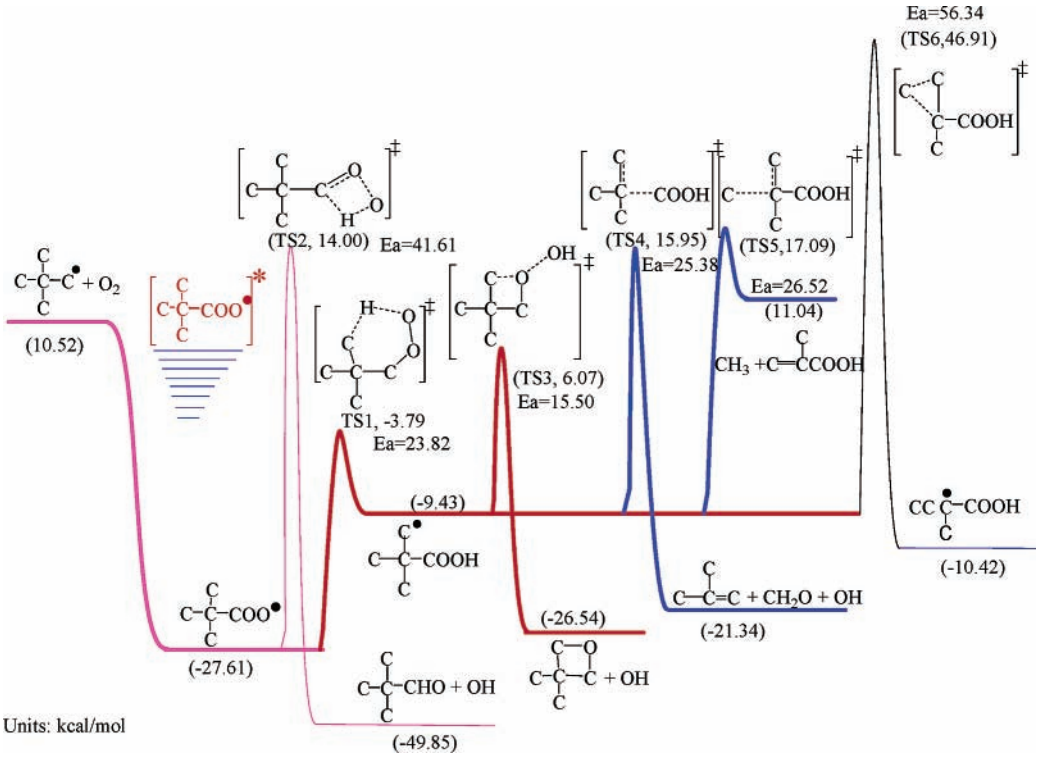

Figure 4. Potential energy diagram for the $C_3CC^{\bullet} + O_2$ reaction system.

SCHEME 2

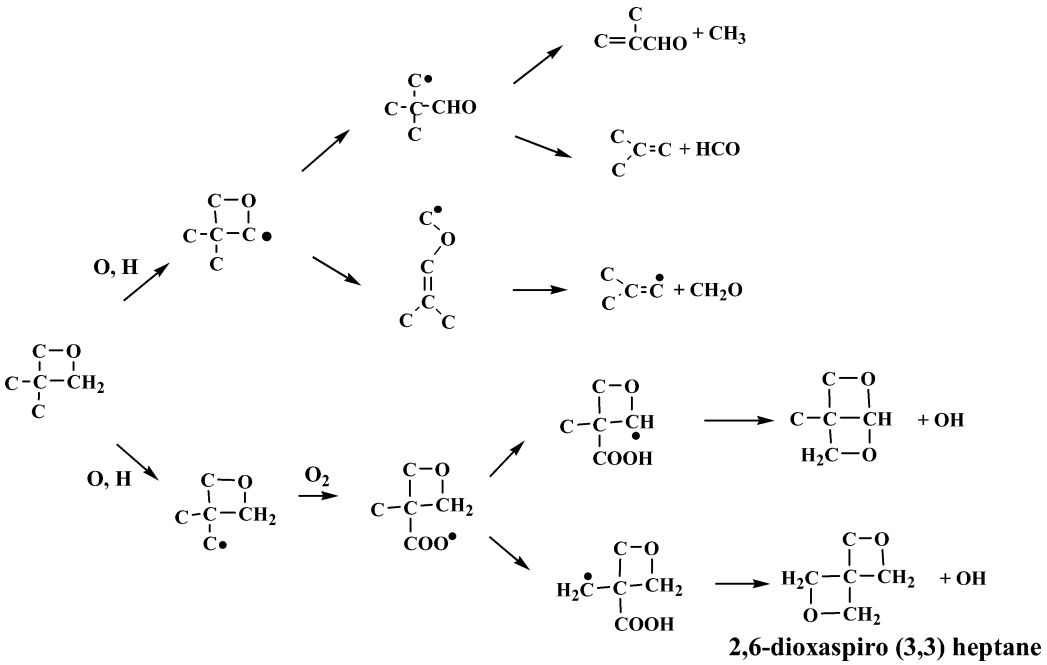

bonded on a carbon in the ring structure or lose a H atom on one of the methyl groups as shown in Scheme 2. The radical generated on a ring carbon will undergo ring opening via C—O bond cleavage to form the C_3•CCHO radical with a barrier[51] of ca. 15 kcal mol^{-1} or via C—C bond cleavage to form C_2C═COC• (E_a = 33.13 kcal/mol). The C_3•CCHO radical undergoes β-scission leading to the formation of isobutene + HCO (E_a = 18.77 kcal/mol) or methacrolein + CH_3 (E_a = 27.33 kcal/mol).

The C_2C═COC• radical undergoes β-scission to form CH_2O plus the C_2C═C• vinylic radical (E_a = 32.33 kcal/mol). This isobutenyl vinyl radical will rapidly undergo further oxidation,[52] the addition of O_2 to form the peroxy radical.

The primary methyl radical can also react with O_2 to form a peroxy radical and then isomerize by a H shift with a ca. 22 kcal mol^{-1} barrier to a hydroperoxy alkyl radical. The alkyl radical will add to the −COOH peroxide oxygen and undergo OH elimination to form 2,6-dioxaspiro (3,3) heptane and its isomer (Scheme 2).

The high-pressure-limit rate constants for the $C_3CC^{\bullet} + O_2$ system are calculated from canonical transition-state theory and fit by three parameters A_∞, n, and E_a over the temperature range from 298 to 2000 K, $k_\infty = AT^n \exp(-E_a/RT)$, by the THERMKIN[53] program. These kinetic parameters are used as input for QRRK and master equation analysis. Thermodynamic analyses

TABLE 6: Kinetic Parameters for $C_3CC^{\bullet} + O_2$ System[a]

	$T = 300-900$ K			$T = 900-2500$ K			
	A	n	E_a[b]	A	n	E_a	P (atm)
$C_3CC^{\bullet} + O_2 \rightarrow C_3CCOO^{\bullet}$	2.376×10^{83}	−21.68	8480	8.315×10^{31}	−5.70	−8990	k_0[c]
$C_3CC^{\bullet} + O_2 \rightarrow C_3CCOO^{\bullet}$	5.97×10^{83}	−24.04	16782	2.37×10^{122}	−37.03	18 134	0.0001
$C_3CC^{\bullet} + O_2 \rightarrow C_3CCOO^{\bullet}$	1.98×10^{59}	−15.87	10959	2.26×10^{132}	−39.34	26 563	0.01
$C_3CC^{\bullet} + O_2 \rightarrow C_3CCOO^{\bullet}$	1.30×10^{36}	−8.24	5020	3.96×10^{147}	−43.02	40 821	0.1
$C_3CC^{\bullet} + O_2 \rightarrow C_3CCOO^{\bullet}$	3.84×10^{22}	−3.82	1429	4.86×10^{168}	−48.27	61 586	1
$C_3CC^{\bullet} + O_2 \rightarrow C_3CCOO^{\bullet}$	1.48×10^{18}	−2.38	237	8.68×10^{192}	−54.40	86 257	10
$C_3CC^{\bullet} + O_2 \rightarrow C_3CCOO^{\bullet}$	1.990×10^{17}	−2.10	0	1.990×10^{17}	−2.10	0	k_∞
$C_3CC^{\bullet} + O_2 \rightarrow C_3CCHO + OH$	1.481×10^{4}	1.73	3960	1.934×10^{15}	−1.66	8580	k_0
$C_3CC^{\bullet} + O_2 \rightarrow C_3CCHO + OH$	4.13×10^{25}	−4.77	13 354	1.19×10^{22}	−3.61	12 928	0.0001
$C_3CC^{\bullet} + O_2 \rightarrow C_3CCHO + OH$	3.18×10^{23}	−3.92	14 728	1.72×10^{22}	−3.65	13 076	0.01
$C_3CC^{\bullet} + O_2 \rightarrow C_3CCHO + OH$	1.37×10^{7}	1.38	11 667	3.94×10^{23}	−4.02	14 351	0.1
$C_3CC^{\bullet} + O_2 \rightarrow C_3CCHO + OH$	7.21×10^{-14}	7.76	6888	4.14×10^{30}	−5.92	20 973	1
$C_3CC^{\bullet} + O_2 \rightarrow C_3CCHO + OH$	4.94×10^{-26}	11.42	3954	1.40×10^{47}	−10.38	37 096	10
$C_3CC^{\bullet} + O_2 \rightarrow C_3CCHO + OH$	4.442×10^{-36}	13.24	1480	3.440×10^{9}	−0.51	19 080	k_∞[d]
$C_3CC^{\bullet} + O_2 \rightarrow C_3^{\bullet}CCOOH$	3.035×10^{54}	−12.75	2440	1.219×10^{45}	−9.74	140	k_0[c]
$C_3CC^{\bullet} + O_2 \rightarrow C_3^{\bullet}CCOOH$	1.25×10^{84}	−26.03	14 321	1.11×10^{112}	−35.60	13 051	0.0001
$C_3CC^{\bullet} + O_2 \rightarrow C_3^{\bullet}CCOOH$	4.57×10^{98}	−30.13	20 350	1.19×10^{120}	−37.43	19 205	0.01
$C_3CC^{\bullet} + O_2 \rightarrow C_3^{\bullet}CCOOH$	4.12×10^{112}	−33.93	27 806	2.80×10^{130}	−39.84	28 697	0.1
$C_3CC^{\bullet} + O_2 \rightarrow C_3^{\bullet}CCOOH$	5.72×10^{103}	−30.66	28 315	3.46×10^{141}	−42.46	40 292	1
$C_3CC^{\bullet} + O_2 \rightarrow C_3^{\bullet}CCOOH$	1.40×10^{76}	−21.62	22 560	1.62×10^{151}	−44.78	51 132	10
$C_3CC^{\bullet} + O_2 \rightarrow C_3^{\bullet}CCOOH$	6.680×10^{-27}	10.35	−4220	3.760×10^{11}	−1.31	9370	k_∞[d]
$C_3CC^{\bullet} + O_2 \rightarrow C_2CYCCOC + OH$	2.509×10^{22}	−3.80	1250	6.467×10^{26}	−5.19	2550	k_0
$C_3CC^{\bullet} + O_2 \rightarrow C_2CYCCOC + OH$	2.30×10^{49}	−11.80	14 954	2.89×10^{13}	−1.39	−6225	0.0001
$C_3CC^{\bullet} + O_2 \rightarrow C_2CYCCOC + OH$	7.46×10^{43}	−9.84	16 056	8.65×10^{13}	−1.51	−5790	0.01
$C_3CC^{\bullet} + O_2 \rightarrow C_2CYCCOC + OH$	4.37×10^{30}	−5.44	15 368	3.71×10^{17}	−2.50	−2449	0.1
$C_3CC^{\bullet} + O_2 \rightarrow C_2CYCCOC + OH$	9.53×10^{6}	2.12	11 344	1.13×10^{30}	−5.89	9210	1
$C_3CC^{\bullet} + O_2 \rightarrow C_2CYCCOC + OH$	3.52×10^{-24}	11.64	4717	2.61×10^{51}	−11.66	30 021	10
$C_3CC^{\bullet} + O_2 \rightarrow C_2CYCCOC + OH$	3.537×10^{-39}	13.36	220	2.884×10^{-2}	1.79	11 540	k_∞[e]
$C_3CC^{\bullet} + O_2 \rightarrow C_2C{=}C + CH_2O + OH$	6.695×10^{22}	−3.86	9740	1.826×10^{26}	−4.93	10 950	k_0
$C_3CC^{\bullet} + O_2 \rightarrow C_2C{=}C + CH_2O + OH$	1.48×10^{40}	−9.11	17 369	2.29×10^{22}	−3.82	8372	0.0001
$C_3CC^{\bullet} + O_2 \rightarrow C_2C{=}C + CH_2O + OH$	1.55×10^{42}	−9.54	20 402	3.85×10^{22}	−3.88	8583	0.01
$C_3CC^{\bullet} + O_2 \rightarrow C_2C{=}C + CH_2O + OH$	1.23×10^{34}	−6.73	21 164	2.46×10^{24}	−4.37	10 274	0.1
$C_3CC^{\bullet} + O_2 \rightarrow C_2C{=}C + CH_2O + OH$	2.82×10^{12}	0.24	17 880	5.90×10^{32}	−6.64	18 174	1
$C_3CC^{\bullet} + O_2 \rightarrow C_2C{=}C + CH_2O + OH$	1.17×10^{-18}	9.76	11 290	4.34×10^{51}	−11.74	36 518	10
$C_3CC^{\bullet} + O_2 \rightarrow C_2C{=}C + CH_2O + OH$	1.548×10^{-37}	12.92	6350	2.917×10^{-1}	1.60	18 000	k_∞[e]
$C_3CC^{\bullet} + O_2 \rightarrow C{=}C(C)CQOH + CH_3$	2.982×10^{21}	−3.45	10 520	3.880×10^{24}	−4.42	11 640	k_0
$C_3CC^{\bullet} + O_2 \rightarrow C{=}C(C)CQOH + CH_3$	5.52×10^{37}	−8.38	17 620	2.82×10^{21}	−3.53	9553	0.0001
$C_3CC^{\bullet} + O_2 \rightarrow C{=}C(C)CQOH + CH_3$	2.10×10^{40}	−8.98	20 778	4.54×10^{21}	−3.58	9747	0.01
$C_3CC^{\bullet} + O_2 \rightarrow C{=}C(C)CQOH + CH_3$	5.10×10^{32}	−6.34	21 667	2.21×10^{23}	−4.04	11 327	0.1
$C_3CC^{\bullet} + O_2 \rightarrow C{=}C(C)CQOH + CH_3$	2.42×10^{11}	0.54	18 490	2.65×10^{31}	−6.23	18 944	1
$C_3CC^{\bullet} + O_2 \rightarrow C{=}C(C)CQOH + CH_3$	1.14×10^{-19}	10.05	11 927	1.11×10^{50}	−11.26	37 048	10
$C_3CC^{\bullet} + O_2 \rightarrow C{=}C(C)CQOH + CH_3$	6.035×10^{-39}	13.35	6930	7.135×10^{-3}	2.09	18 500	k_∞[e]
$C_3CC^{\bullet} + O_2 \rightarrow CCC^{\bullet}(C)COOH$	1.215×10^{21}	−3.53	40 170	2.399×10^{23}	−4.20	41 410	k_0
$C_3CC^{\bullet} + O_2 \rightarrow CCC^{\bullet}(C)COOH$	1.10×10^{21}	−3.51	40 153	1.96×10^{58}	−14.28	62 589	0.0001
$C_3CC^{\bullet} + O_2 \rightarrow CCC^{\bullet}(C)COOH$	1.96×10^{21}	−3.59	40 252	1.96×10^{58}	−14.28	62 590	0.01
$C_3CC^{\bullet} + O_2 \rightarrow CCC^{\bullet}(C)COOH$	4.64×10^{27}	−5.53	42 992	2.01×10^{58}	−14.29	62 600	0.1
$C_3CC^{\bullet} + O_2 \rightarrow CCC^{\bullet}(C)COOH$	2.78×10^{30}	−6.17	46 483	4.31×10^{58}	−14.38	62 909	1
$C_3CC^{\bullet} + O_2 \rightarrow CCC^{\bullet}(C)COOH$	9.00×10^{9}	0.48	43 584	2.43×10^{64}	−15.94	68 347	10
$C_3CC^{\bullet} + O_2 \rightarrow CCC^{\bullet}(C)COOH$	4.879×10^{-28}	9.93	35 490	6.547×10^{-3}	1.90	41 190	k_∞[e]
$C_3CCOO^{\bullet} \rightarrow C_3CCHO + OH$	5.328×10^{58}	−13.29	47 210	2.766×10^{24}	−2.66	35 390	k_0[c]
$C_3CCOO^{\bullet} \rightarrow C_3CCHO + OH$	5.04×10^{86}	−24.90	59 745	4.81×10^{49}	−14.41	34 774	0.0001
$C_3CCOO^{\bullet} \rightarrow C_3CCHO + OH$	2.82×10^{58}	−15.18	53 986	8.06×10^{48}	−13.09	40 627	0.01
$C_3CCOO^{\bullet} \rightarrow C_3CCHO + OH$	5.05×10^{30}	−5.96	47 207	5.98×10^{58}	−15.02	52 983	0.1
$C_3CCOO^{\bullet} \rightarrow C_3CCHO + OH$	5.02×10^{14}	−0.71	43 050	1.26×10^{53}	−12.65	55 846	1
$C_3CCOO^{\bullet} \rightarrow C_3CCHO + OH$	2.01×10^{9}	1.05	41 609	3.79×10^{62}	−14.62	70 229	10
$C_3CCOO^{\bullet} \rightarrow C_3CCHO + OH$	1.286×10^{8}	1.42	41 080	2.362×10^{7}	1.57	39 970	k_∞
$C_3CCOO^{\bullet} \rightarrow C_3^{\bullet}CCOOH$	7.672×10^{60}	−14.64	30 360	1.101×10^{141}	−38.26	73 330	k_0[c]
$C_3CCOO^{\bullet} \rightarrow C_3^{\bullet}CCOOH$	2.14×10^{35}	−7.93	30 647	5.04×10^{30}	−7.15	21 179	0.0001
$C_3CCOO^{\bullet} \rightarrow C_3^{\bullet}CCOOH$	3.27×10^{21}	−3.37	27 174	4.96×10^{30}	−6.67	25 011	0.01
$C_3CCOO^{\bullet} \rightarrow C_3^{\bullet}CCOOH$	7.95×10^{11}	−0.22	24 645	2.88×10^{37}	−8.21	32 793	0.1
$C_3CCOO^{\bullet} \rightarrow C_3^{\bullet}CCOOH$	8.87×10^{7}	1.07	23 582	1.44×10^{35}	−7.20	34 953	1
$C_3CCOO^{\bullet} \rightarrow C_3^{\bullet}CCOOH$	1.09×10^{7}	1.36	23 334	3.86×10^{37}	−7.55	40 733	10
$C_3CCOO^{\bullet} \rightarrow C_3^{\bullet}CCOOH$	2.782×10^{6}	1.54	23010	2.074×10^{140}	−34.58	68 030	k_∞
$C_3^{\bullet}CCOOH \rightarrow C_2CYCCOC + OH$	1.615×10^{49}	−10.63	17 130	9.778×10^{21}	−2.19	7410	k_0[c]
$C_3^{\bullet}CCOOH \rightarrow C_2CYCCOC + OH$	2.17×10^{55}	−15.02	26 010	1.05×10^{9}	−1.06	4775	0.0001
$C_3^{\bullet}CCOOH \rightarrow C_2CYCCOC + OH$	1.86×10^{58}	−15.51	27 938	3.52×10^{11}	−1.47	6095	0.01
$C_3^{\bullet}CCOOH \rightarrow C_2CYCCOC + OH$	2.66×10^{44}	−10.60	25 563	2.86×10^{30}	−6.43	17 906	0.1
$C_3^{\bullet}CCOOH \rightarrow C_2CYCCOC + OH$	3.05×10^{35}	−7.46	23 987	4.78×10^{17}	−2.45	11 497	1
$C_3^{\bullet}CCOOH \rightarrow C_2CYCCOC + OH$	3.38×10^{25}	−4.15	21 548	3.56×10^{23}	−3.82	17 451	10
$C_3^{\bullet}CCOOH \rightarrow C_2CYCCOC + OH$	6.636×10^{8}	1.06	15 360	4.032×10^{6}	1.71	14 110	k_∞

TABLE 6 (Continued)

	$T = 300-900$ K			$T = 900-2500$ K			
	A	n	E_a [b]	A	n	E_a	P (atm)
C_3•CCOOH → C_2C=C + CH_2O + OH	4.997×10^{31}	−4.83	25 590	6.968×10^{30}	−4.43	26 750	k_0 [c]
C_3•CCOOH → C_2C=C + CH_2O + OH	1.55×10^{58}	−18.15	29 519	2.98×10^{0}	−0.76	3084	0.0001
C_3•CCOOH → C_2C=C + CH_2O + OH	6.75×10^{75}	−22.52	36 727	6.06×10^{17}	−5.12	8985	0.01
C_3•CCOOH → C_2C=C + CH_2O + OH	4.94×10^{59}	−16.10	35 902	1.94×10^{49}	−13.03	29 281	0.1
C_3•CCOOH → C_2C=C + CH_2O + OH	6.04×10^{45}	−10.95	34 330	6.31×10^{27}	−6.12	19 121	1
C_3•CCOOH → C_2C=C + CH_2O + OH	7.82×10^{24}	−3.96	29 417	3.58×10^{36}	−7.99	28 571	10
C_3•CCOOH → C_2C=C + CH_2O + OH	1.146×10^{11}	0.57	25 680	8.182×10^{8}	1.20	24 480	k_∞
C_3•CCOOH → C=C(C)CQOH + CH_3	3.487×10^{29}	−4.16	26 280	2.600×10^{29}	−3.99	27 770	k_0 [c]
C_3•CCOOH → C=C(C)CQOH + CH_3	3.08×10^{56}	−17.84	29 804	7.76×10^{-3}	−0.18	3017	0.0001
C_3•CCOOH → C=C(C)CQOH + CH_3	7.52×10^{75}	−22.69	37 525	2.24×10^{16}	−4.85	9026	0.01
C_3•CCOOH → C=C(C)CQOH + CH_3	8.57×10^{59}	−16.26	36 936	1.11×10^{49}	−13.05	30 100	0.1
C_3•CCOOH → C=C(C)CQOH + CH_3	6.17×10^{45}	−11.00	35 431	8.72×10^{26}	−5.92	19 710	1
C_3•CCOOH → C=C(C)CQOH + CH_3	1.07×10^{24}	−3.71	30 332	6.77×10^{35}	−7.80	29 382	10
C_3•CCOOH → C=C(C)CQOH + CH_3	3.110×10^{9}	1.05	26 430	2.349×10^{7}	1.67	25 230	k_∞
C_3•CCOOH → CCC•(C)COOH	2.321×10^{21}	−1.80	55 410	8.359×10^{29}	−4.20	61 320	k_0 [c]
C_3•CCOOH → CCC•(C)COOH	8.48×10^{14}	−13.08	44 176	7.71×10^{-32}	0.89	24 172	0.0001
C_3•CCOOH → CCC•(C)COOH	1.26×10^{80}	−32.10	53 259	2.81×10^{-19}	−2.43	7224	0.01
C_3•CCOOH → CCC•(C)COOH	4.04×10^{133}	−44.85	73 455	2.34×10^{57}	−22.25	32 416	0.1
C_3•CCOOH → CCC•(C)COOH	3.37×10^{128}	−39.60	81 938	5.76×10^{69}	−22.63	46 351	1
C_3•CCOOH → CCC•(C)COOH	4.18×10^{71}	−19.60	71 555	1.23×10^{80}	−23.05	65 121	10
C_3•CCOOH → CCC•(C)COOH	6.718×10^{10}	0.57	56 410	5.967×10^{8}	1.16	55 250	k_∞

[a] Geometric mean frequency from CPFIT (Ritter, E. R. *J. Chem. Inf. Comput. Sci.* **1991**, *31*, 400). [b] C_3CCOO•: 446.0 cm^{-1} (17.502), 1385.3 cm^{-1} (19.421), 3480.2 cm^{-1} (8.577). C_3•CCOOH: 403.1 cm^{-1} (17.879), 1388.0 cm^{-1} (18.733), 3466.4 cm^{-1} (8.388). Lennard-Jones parameters: $\sigma = 5.86$ Å, $\epsilon/k = 632$ K. [b]Units for A in s^{-1} or cm^3 mol^{-1} s^{-1} and units for E_a in cal mol^{-1}. [c] Low-pressure limit: multiply rate by [M]. [d] High-pressure limit: multiply rate by $[M]^{-1}$. [e] High-pressure limit: multiply rate by $[M]^{-2}$.

for reactions of neopentyl oxidation by the THERMKIN are illustrated in Table S3. Table 6 lists the calculated rate constants as a function of temperature for the low- and high-pressure-limit cases and for specific pressures of 0.001, 0.01, 0.1, 1, and 10 atm. These rate constants are presented in two temperature ranges, 300−900 K and 900−2500 K, to reduce the nonlinear Arrhenius fit deviation to an acceptable range.

We also present the calculated rate constant data in a combined pressure and temperature form of Chebyshev polynomials[54] and report this in Supporting Information (Table S5). We tried to fit less complex falloff expressions to the data, but because of the many product channels involved, the deviations in the observed fits were unacceptable and often more than 100%. The expressions yielded satisfactory agreement only in single-well, single-product dissociations, where the depletion of higher-energy-level populations by lower barrier reactions was not occurring. These expressions included Troe's F_{cent} method,[30] the SRI method,[55] and the extended Troe's F_{cent} method.[56] These have been previously tried on mutiple-well, multiple-product, chemically activated or dissociation reactions and were reported to be unsatisfactory.[57] Tsang[58] recently studied the multi-channel decomposition of ethanol, and indicated that the Troe formalism does not work for rate constant fits vs pressure over a wide pressure range when the unimolecular decomposition has multiple channels. The lower energy channels deplete the higher energy states and significantly change the falloff behavior of the higher energy reaction processes. Venkatesh et al.[54] reported that a direct approximation of the rate coefficients via Chebyshev expansions yields reliable and accurate representations of the pressure−temperature behavior. Venkatesh et al.[54] also reported that these Chebyshev fits are superior to using a Lindemann-based approach to fit the form factor representing the falloff surface.

The data in Table S5 represent our predicted kinetic parameters in the form of 9 × 5 Chebyshev polynomials[54] at pressures of 0.001−100 atm and temperatures of 300−2500 K with a master equation analysis to account for intermolecular energy transfer. The average errors for the 9 × 5 parameter Chebyshev fit are also listed in Table S5. These approximated Chebyshev polynomials are compatible with those of Chemkin[59,60] for the use of simulation and the modeling combustion process.

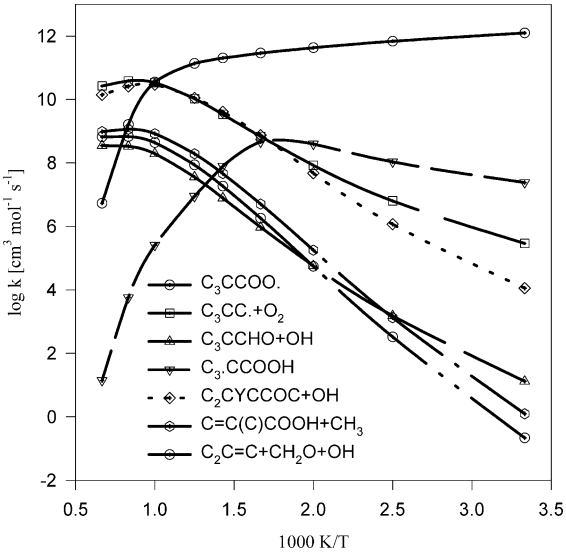

Figure 5. Calculated temperature-dependent rate constants for the chemically activated C_3CC• + O_2 system at $P = 1$ atm.

The calculated temperature-dependent rate constants for the chemically activated C_3CC• + O_2 reaction system from 300 to 1500 K at 1 atm are illustrated in Figure 5. The dominant product channel for C_3CC• + O_2 is stabilization to C_3CCOO• below 1000 K. The forward and reverse isomerization and reverse reaction dissociation occur rapidly; the isomerization and the epoxide-formation steps have relatively tight transition states with Arrhenius preexponential factors of ca. 10^{11} s^{-1} between 300−800 K, and the reverse isomerization is fast because of the very low barrier (5.64 kcal mol^{-1}). At low temperatures of 600−700 K, the stabilization and isomerization are the dominant channels; the reverse reaction and dissociation

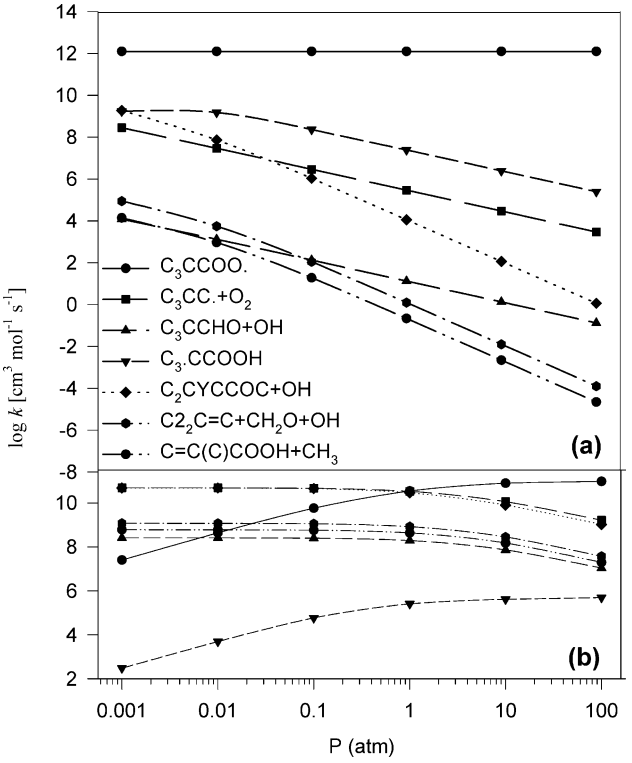

Figure 6. Calculated pressure-dependent rate constants for the chemically activated $C_3CC^{\bullet} + O_2$ system. (a) $T = 300$ K, (b) $T = 1000$ K.

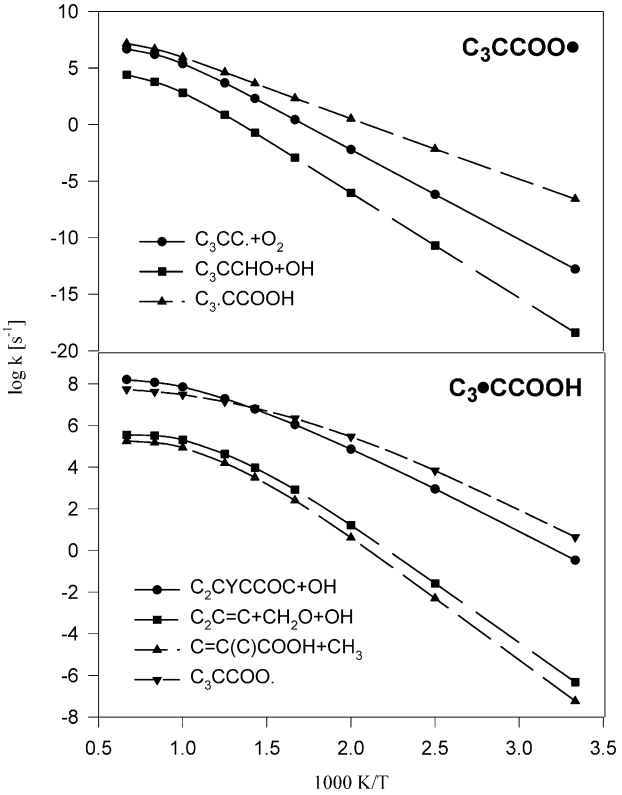

Figure 7. Calculated temperature-dependent dissociation rate constants for $C_3CCOO^{\bullet}$ and $C_3^{\bullet}CCOOH$ at $P = 1$ atm.

to 3,3-dimethyloxetane + OH are the important reactions above 900 K, and this results in falloff by 900 K.

Figure 6 illustrates the pressure dependence for the rate constants (log k vs P) of the chemically activated reactions at 300 and 1000 K. Stabilization to $C_3CCOO^{\bullet}$ is the dominant channel over all pressures at 300 K; it is also the dominant product channel when the pressure is greater than 1 atm at 1000 K. The rate of formation of $C_3^{\bullet}CCOOH$ from chemical activation appears to be higher at low temperature, 94.6 times higher at 300 K than at 1000 K, 1 atm. This is because the stabilization to $C_3CCOO^{\bullet}$ decreases significantly at 1000 K relative to that at 300 K, and the rates of dissociation to neopentyl + O_2 and DMO + OH are near equal and much faster at 1000 K (Figure 6b). The importance of the isomerization reaction for low-temperature hydrocarbon oxidation can be seen here.

When the pressure is below 1 atm, the dissociation back to $C_3CC^{\bullet} + O_2$ becomes the dominant channel at 1000 K, with the formation of 3,3-dimethyloxetane + OH competitive over the entire temperature range. The rate constants of other dissociation channels decrease as the pressure increases. The next important reactions are the formation of isobutene + CH_2O + OH and C═C(C)COOH + CH_3, which have similar rates and are lower than the epoxide + OH channel over the entire pressure range.

3.2. Dissociation/Isomerization of the Neopentyl Peroxy and Hydroperoxide-Neopentyl Isomers. The stabilization of the neopentyl peroxy adduct is an important product in the chemical activation reaction system below 1000 K. The plot of log k vs $1/T$ for the reaction channels of the stabilized $C_3CCOO^{\bullet}$ radical at atmospheric pressure is shown in Figure 7. The isomerization to $C_3^{\bullet}CCOOH$ is the fastest channel in all temperature ranges, and the dissociation back to reactants $C_3CC^{\bullet} + O_2$ is competitive with the isomerization above 800 K. The isomer $C_3^{\bullet}CCOOH$ has a very low barrier (5.64 kcal/mol) for reverse reaction, which is therefore fast; the neopentyl peroxy radical and the hydroperoxy-neopentyl isomer will exist in a quasi-equilibrium, where the lower-enthalpy peroxy radical will be the dominant isomer. The four important reactions of the stabilized $C_3^{\bullet}CCOOH$ radical at atmospheric pressure are also shown in Figure 7. The fastest channel is the isomerization back to $C_3CCOO^{\bullet}$, but dissociation to 3,3-dimethyloxetane + OH, which has a barrier of 15.50 kcal/mol, is competitive with this reverse isomerization over the entire temperature range because of a higher preexponential factor. The reaction channels for dissociation to C$_2$C═C + CH_2O + OH and dissociation to C═C(C)COOH + CH_3 are similar and several orders of magnitude lower than that of the epoxide + OH channel from 300−1500 K.

We note that the master equation analysis[6] for isomerization or dissociation from stabilized adducts does not include reactions past the adjacent well(s). We account for the further reaction of these products in the numerical kinetic integration (Chemkin analysis).

3.3. $C_3^{\bullet}CCOOH + O_2$. The potential energy surface for the addition of a second O_2 to the hydroperoxy-neopentyl radical ($C_3^{\bullet}CCOOH$) calculated at the B3LYP/6-311++G(3df,2p) level is shown in Figure 8. $C_3^{\bullet}CCOOH$ reacts with O_2 to form a hydroperoxide-peroxy $C_2C(OOH)COO^{\bullet}$ with a 32.96 kcal mol^{-1} well depth. Reaction channels for the chemically activated adduct $C_2C(OOH)COO^*$ include dissociation back to reactants, stabilization to $C_2C(OOH)COO^{\bullet}$, isomerization via a hydrogen shift via TS7 ($E_a = 22.58$ kcal mol^{-1}) to form a dihydroperoxide isomer $C_2^{\bullet}C(COOH)_2$ ($\Delta H_{f^\circ 298} = -25.14$ kcal mol^{-1}), and dissociation to products ($C_2C(OOH)CHO$ + OH) via two different transition states, TS8 ($E_a = 22.40$ kcal mol^{-1}) and TS8A ($E_a = 41.23$ kcal mol^{-1}). The dihydroperoxide isomer $C_2^{\bullet}C(COOH)_2$ undergoes dissociation to 3-methyl,3-hydroperoxideoxetane + OH via TS9 ($E_a = 14.35$ kcal mol^{-1}) and β-scission to generate a hydroperoxide olefin C═C(C)COOH and CH_2O + OH via TS10 ($E_a = 17.34$ kcal mol^{-1}). The

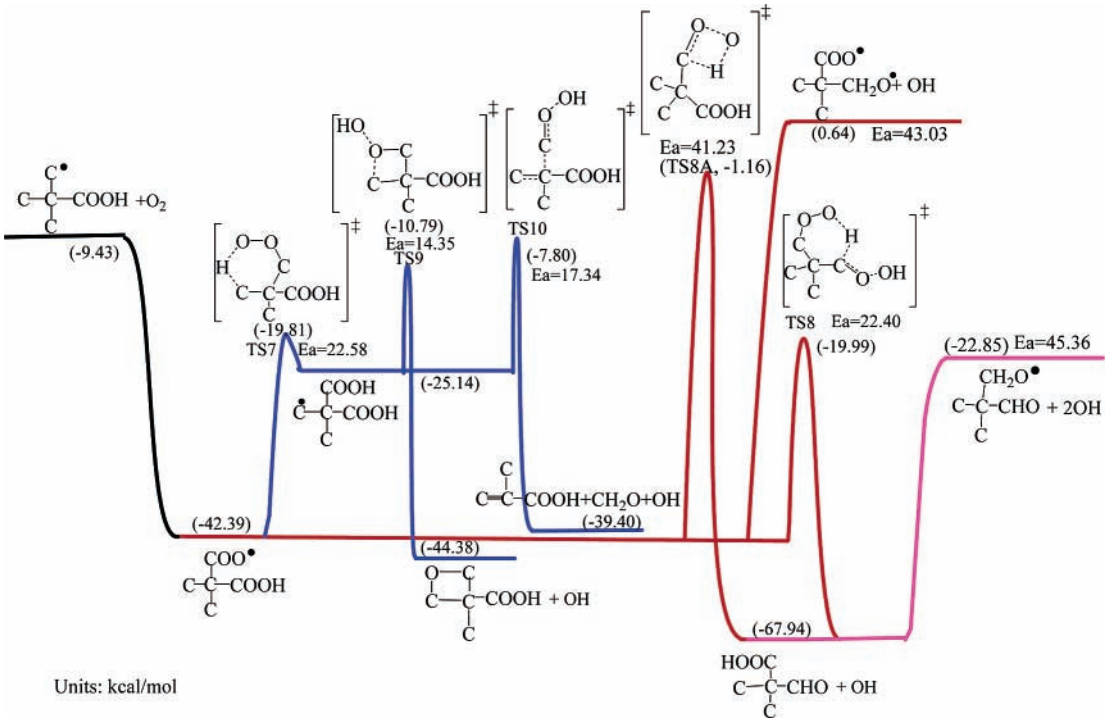

Figure 8. Potential energy diagram for the C_3•CCOOH + O_2 reaction system.

TABLE 7: Comparison and Estimation of Reaction Enthalpies for Similar Channels[a]

	B3LYP /6-31G(d,p)	B3LYP /6-311++G(3df,2p)	CBSQ//B3LYP /6-31G(d,p)		B3LYP /6-31G(d,p)	B3LYP /6-311++G(3df,2p)	corrected[b]
TS1	24.00	23.42	23.82	TS7	22.79	22.58	22.98
TS2	42.54	42.06	41.61	TS8A	41.87	41.26	40.78
TS3	14.71	14.14	15.51	TS9	15.86	14.35	15.72
TS4	29.97	27.81	25.39	TS10	19.28	17.34	14.93
				TS8	22.93	22.40	

[a] kcal/mol. [b] Corrected reaction enthalpies according to the trend calculated from three different levels for the similar reaction channels.

stabilized $C_2C(OOH)COO^{\bullet}$ peroxy undergoes homolytic dissociation via cleavage of the weak O—O bond with a barrier of 43.03 kcal mol^{-1}. The stable vinyl hydroperoxide that is produced will also undergo homolytic cleavage of the weak O—O bond in the peroxide moiety to generate OH and a vinyl alkoxy (chain-branching reaction), serving to accelerate the oxidation process. The vinyl alkoxy radical is an important reaction to form 2-methyl-2-propenal (C=C(C)CHO), which was identified as an important product from neopentyl radical oxidation.[9]

A number of the reaction channels for the $C_2C(COOH)COO^{\bullet}$* adduct are similar to those of the $C_3CCOO^{\bullet}$* adduct because of the similarity between the two adduct structures. Table 7 lists calculated reaction enthalpies for similar reaction channels in Figures 4 and 8. In Table 7, the barriers for the corresponding isomerization channels and dissociation channels in two reaction systems show agreement, especially for the channels with tight transition states (ring formation).

To obtain reaction enthalpies in this second O_2 addition system that are more accurate than those from the DFT calculations, we evaluate the deviation of enthalpies between the DFT and the CBS-Q levels and then correct the corresponding DFT-level reaction enthalpies to the CBS-Q level for these oxygenated species. The barriers calculated from the B3LYP/6-311++G(3df,2p) level in Figure 8 are corrected to 22.98, 15.72, 14.93, and 40.78 kcal mol^{-1} for TS7, TS9, TS10, and TS8A, respectively. The correction is 0.4−1.4 kcal mol^{-1} for the reactions with ring-formation transition states and 2.4 kcal mol^{-1} for the dissociation of the $-CH_2OOH$ group with TS10.

One new important channel in Figure 8 that is not in the $C_3CC^{\bullet}$ + O_2 system (Figure 4) is the exothermic formation of $C_2C(COOH)CHO$ + OH via a six-membered-ring transition state (TS8) with a 22.40 kcal mol^{-1} barrier. In TS8, the peroxy radical abstracts the weakly bonded H atom in the $-CH_2OOH$ group; this H—$C(C_2)$HOOH bond is weak because as the H atom is leaving a strong carbonyl bond (gain of ~80 kcal mol^{-1}) is forming with the weak O—OH bond (~45 kcal mol^{-1}) cleaving.

The chemically activated $[C_2C(COOH)CHO]^*$ species can undergo dissociation to cleave the weak RO—OH bond to form a 2-methyl isopropanal-2-methyoxy radical ($C_2C(CHO)CH_2O^{\bullet}$) plus a second OH (overall reaction $C_3^{\bullet}CCOOH + O_2 \rightarrow C_2C(CHO)CH_2O^{\bullet} + 2OH$), or it can be stabilized. Although the branching ratio to the two products is a function of temperature, we calculate it to be near 1:1 for the conditions modeled in this study. The $[C_2C(COOH)CHO]^*$ species has an activation energy of ca. 48 kcal mol^{-1} at the transition-state point.

The stabilized $C_2C(COOH)CHO$ can undergo bimolecular reaction (loss of H atoms via abstraction) and the product radicals can dissociate by low-energy β-scission. For example, the weakly bonded H atom will be abstracted to form the $C_2C(COOH)C^{\bullet}$=O radical, which will dissociate to CO and $C_2C^{\bullet}COOH$; the $C_2C^{\bullet}COOH$ will further dissociate to isobutene + HO_2. These are important chain-branching channels at low temperature, and they also contribute to OH and HO_2 product formation.

The 2-methyl isopropanal-2-methyoxy radical $C_2C(CHO)CH_2O^{\bullet}$ will undergo β-scission either to $C_2C^{\bullet}(CHO)$ + CH_2O

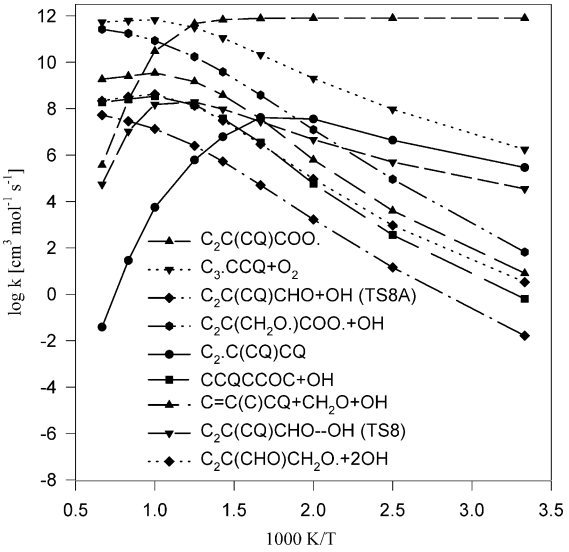

Figure 9. Calculated temperature-dependent rate constants for the chemically activated C_3•CCOOH + O_2 system at $P = 1$ atm.

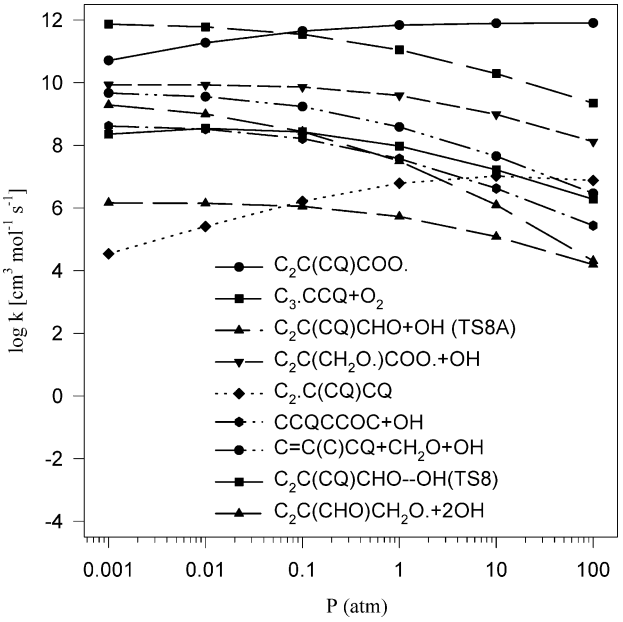

Figure 10. Calculated pressure-dependent rate constants for the chemically activated C_3•CCOOH + O_2 system at $T = 700$ K.

via TS11 or to $C_2C(CHO)_2$ + H via TS12, as outlined in the reaction mechanism scheme. The C_2C•(CHO) radical will undergo β-scission to C═CC + HCO via TS13A or C═C(C)-CHO + H via TS13, which are important products that were observed in neopentane oxidation.[17]

The calculated rate constants for C_3•CCOOH + O_2 are listed in Table 8 as a function of temperature for two ranges, 300−900 K and 900−2500 K, along with the corresponding low- and high-pressure-limit k values at pressures of 0.001, 0.01, 0.1, 1, and 10 atm. These rate constants are also listed in Supporting Information Table S5, where they are expressed in a 9 × 5 Chebyshev polynomial format[54] over the temperature range of 300−2500 K and the pressure range of 0.001−100 atm. This Chebyshev representation is compatible with the Chemkin III mechanism integration code.

Temperature-dependent rate constants for the chemically activated C_3•CCOOH + O_2 system are illustrated in Figure 9 for conditions of 300 to 1500 K at 1 atm. The dominant product for C_3•CCOOH + O_2 is stabilization to $C_2C(OOH)COO$• below 800 K, but the reverse reaction becomes the dominant channel above 800 K.

The most important product channel for the dissociation of the stabilized $C_2C(OOH)COO$• radical at atmospheric pressure is the formation of $[C_2C(COOH)CHO]^*$ + OH via TS8 as shown in Figure 9; this reaction is competitive with the isomerization channel to C_2•$C(COOH)_2$ below 600 K. The dissociation channel (chain branching) of $[C_2C(COOH)CHO]^*$ + OH, which further reacts to produce $C_2C(CO$•$)CHO$ + 2OH, becomes dominant to a small degree above 800 K; it is the important forward channel to products and is an important chain-branching step at low and intermediate temperatures. The isomerization to C_2•C-$(COOH)_2$ is the important forward channel below 600 K, and the homolytic cleavage of the weak RO−OH bond in C_2C-(OOH)COO• (also a chain-branching path) becomes important above 600 K.

A plot of log k versus pressure for the C_3•CCOOH + O_2 system at 700 K is shown in Figure 10, which illustrates that stabilization to the peroxy radical and reverse (dissociation) reaction channels are dominant at all pressures.

4. Unimolecular Dissociation of the Neopentyl Radical. At higher reaction temperatures, the neopentyl radical will undergo unimolecular dissociation to isobutene plus the methyl radical in competition with the R• + O_2 association reaction.

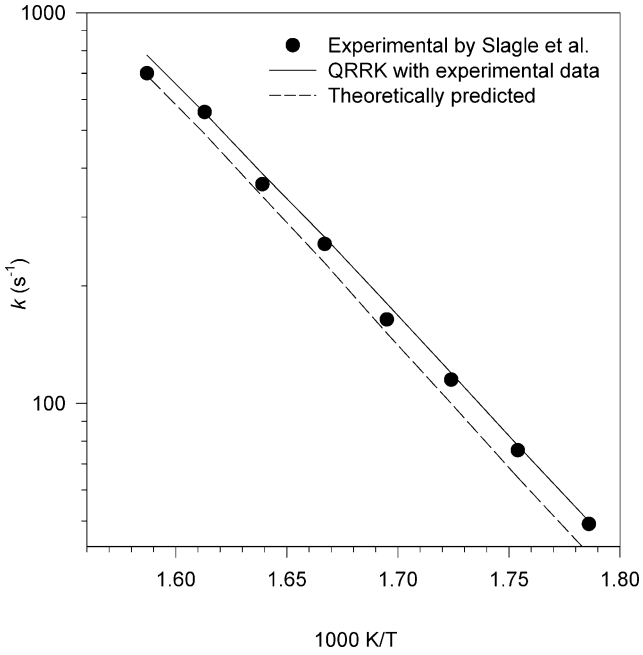

Figure 11. Comparison of calculated unimolecular dissociation constants of the neopentyl radical with the experimental data of Slagle et al.[61]

Slagle et al.[61] studied the unimolecular decomposition of the neopentyl radical ($T = 560-650$ K) in time-resolved experiments by using a heated tubular reactor coupled to a photoionization mass spectrometer. They fit their experimental data to the framework of RRKM theory and a vibrational model and determined high-pressure-limit rate constants in the temperature range to be $k = 10^{13.9}\exp(-30.9 \pm 1.0 \text{ kcal mol}^{-1}/RT)\ \text{s}^{-1}$. In this work, the high-pressure-limit rate constant is calculated via canonical transition-state theory and fit to a three-parameter (A, n, E_a) modified Arrhenius equation over the temperature range of 300−2000 K: $k = 2.21 \times 10^{10}\, T^{1.085}\exp(-29.78 \text{ kcal mol}^{-1}/RT)\ \text{s}^{-1}$. Figure 11 compares this temperature-dependent rate constant from the experimental data of Slagle et al.[61] with our QRRK calculations, and the QRRK results using both the experimentally determined and theoretically predicted high-

TABLE 8: Kinetic Parameters for the C_3•CCOOH + O_2 System[a]

	$T = 300-900$ K			$T = 900-2500$ K			
	A[b]	n	E_a	A	n	E_a	P (atm)
C_3•CCOOH + O_2 → C_2C(COOH)COO•	1.939×10^{87}	−22.71	9640	1.428×10^{35}	−6.60	−9140	k_0[c]
C_3•CCOOH + O_2 → C_2C(COOH)COO•	1.71×10^{90}	−25.87	19 741	3.99×10^{59}	−18.92	−21 407	0.0001
C_3•CCOOH + O_2 → C_2C(COOH)COO•	1.33×10^{71}	−19.43	15 375	5.93×10^{62}	−19.50	−19 267	0.01
C_3•CCOOH + O_2 → C_2C(COOH)COO•	1.77×10^{90}	−12.20	9911	1.19×10^{68}	−20.67	−15 202	0.1
C_3•CCOOH + O_2 → C_2C(COOH)COO•	4.57×10^{29}	−5.78	4785	1.05×10^{78}	−23.10	−6859	1
C_3•CCOOH + O_2 → C_2C(COOH)COO•	2.93×10^{17}	−1.81	1514	1.21×10^{96}	−27.73	8972	10
C_3•CCOOH + O_2 → C_2C(COOH)COO•	8.000×10^{11}	0.00	0	8.000×10^{11}	0.00	0	k_∞
C_3•CCOOH + O_2 → C_2C(COOH)CHO + OH $_{(TS8)}$	2.646×10^{27}	−6.15	1320	8.520×10^{15}	−2.57	−2640	k_0
C_3•CCOOH + O_2 → C_2C(COOH)CHO + OH $_{(TS8)}$	8.11×10^{46}	−11.62	14 600	8.71×10^{-11}	4.98	−17 891	0.0001
C_3•CCOOH + O_2 → C_2C(COOH)CHO + OH $_{(TS8)}$	1.88×10^{34}	−7.48	12 749	2.43×10^{-10}	4.86	−17 479	0.01
C_3•CCOOH + O_2 → C_2C(COOH)CHO + OH $_{(TS8)}$	1.78×10^{14}	−1.06	8470	1.12×10^{-8}	4.40	−15 941	0.1
C_3•CCOOH + O_2 → C_2C(COOH)CHO + OH $_{(TS8)}$	1.25×10^{-8}	5.94	3180	3.22×10^{-3}	2.92	−10 885	1
C_3•CCOOH + O_2 → C_2C(COOH)CHO + OH $_{(TS8)}$	1.85×10^{-25}	11.12	−966	9.07×10^{10}	−0.73	1632	10
C_3•CCOOH + O_2 → C_2C(COOH)CHO + OH $_{(TS8)}$	4.074×10^{-34}	12.52	−2890	7.503×10^{-8}	3.91	630	k_∞[d]
C_3•CCOOH + O_2 → C_2C(COOH)CHO + OH $_{(TS8A)}$	5.637×10^{6}	0.82	9340	2.312×10^{15}	−1.78	13 270	k_0
C_3•CCOOH + O_2 → C_2C(COOH)CHO + OH $_{(TS8A)}$	1.40×10^{22}	−3.88	15 745	2.58×10^{15}	−1.84	12 625	0.0001
C_3•CCOOH + O_2 → C_2C(COOH)CHO + OH $_{(TS8A)}$	5.19×10^{27}	−5.47	19 208	2.61×10^{15}	−1.84	12 629	0.01
C_3•CCOOH + O_2 → C_2C(COOH)CHO + OH $_{(TS8A)}$	2.79×10^{21}	−3.31	19 335	3.34×10^{15}	−1.87	12 729	0.1
C_3•CCOOH + O_2 → C_2C(COOH)CHO + OH $_{(TS8A)}$	1.00×10^{3}	2.63	15 609	6.34×10^{16}	−2.22	13 905	1
C_3•CCOOH + O_2 → C_2C(COOH)CHO + OH $_{(TS8A)}$	6.01×10^{-19}	9.32	10 559	3.78×10^{23}	−4.06	20 158	10
C_3•CCOOH + O_2 → C_2C(COOH)CHO + OH $_{(TS8A)}$	1.733×10^{-39}	14.66	5630	2.045×10^{-9}	4.93	11 230	k_∞[d]
C_3•CCOOH + O_2 → $C_2C(CH_2O•)COO•$ + OH	2.307×10^{15}	−0.59	12 030	1.656×10^{23}	−2.96	15 550	k_0
C_3•CCOOH + O_2 → $C_2C(CH_2O•)COO•$ + OH	7.15×10^{25}	−3.80	16 283	6.99×10^{26}	−4.09	16 709	0.0001
C_3•CCOOH + O_2 → $C_2C(CH_2O•)COO•$ + OH	3.28×10^{33}	−6.07	20 206	7.01×10^{26}	−4.09	16 710	0.01
C_3•CCOOH + O_2 → $C_2C(CH_2O•)COO•$ + OH	3.01×10^{30}	−4.93	21 286	7.93×10^{26}	−4.10	16 759	0.1
C_3•CCOOH + O_2 → $C_2C(CH_2O•)COO•$ + OH	6.26×10^{13}	0.47	18 148	6.31×10^{27}	−4.35	17 587	1
C_3•CCOOH + O_2 → $C_2C(CH_2O•)COO•$ + OH	2.29×10^{-8}	7.25	13 107	3.83×10^{33}	−5.92	22 916	10
C_3•CCOOH + O_2 → $C_2C(CH_2O•)COO•$ + OH	4.681×10^{-30}	12.99	8040	1.577×10^{-1}	3.73	13 000	k_∞[d]
C_3•CCOOH + O_2 → C_2•$C(COOH)_2$	2.416×10^{45}	−9.79	1340	1.341×10^{40}	−8.29	−2350	k_0[c]
C_3•CCOOH + O_2 → C_2•$C(COOH)_2$	7.38×10^{98}	−31.01	19521	7.15×10^{45}	−16.93	−27 731	0.0001
C_3•CCOOH + O_2 → C_2•$C(COOH)_2$	3.83×10^{127}	−39.53	30 567	1.52×10^{47}	−17.02	−27 444	0.01
C_3•CCOOH + O_2 → C_2•$C(COOH)_2$	1.26×10^{140}	−42.86	37 874	3.39×10^{47}	−16.85	−27 458	0.1
C_3•CCOOH + O_2 → C_2•$C(COOH)_2$	2.47×10^{124}	−37.37	36 515	4.11×10^{46}	−16.37	−28 143	1
C_3•CCOOH + O_2 → C_2•$C(COOH)_2$	1.30×10^{92}	−26.79	29 583	5.54×10^{44}	−15.64	−29 078	10
C_3•CCOOH + O_2 → C_2•$C(COOH)_2$	2.392×10^{-33}	12.62	−2800	1.217×10^{-6}	3.87	940	k_∞[d]
C_3•CCOOH + O_2 → C(COOH)CYCCOC + OH	5.540×10^{17}	−2.73	4290	4.171×10^{22}	−4.35	4760	k_0
C_3•CCOOH + O_2 → C(COOH)CYCCOC + OH	6.93×10^{47}	−11.77	18 403	1.26×10^{-1}	2.48	−9103	0.0001
C_3•CCOOH + O_2 → C(COOH)CYCCOC + OH	5.24×10^{51}	−12.71	22 759	1.59×10^{-1}	2.45	−9012	0.01
C_3•CCOOH + O_2 → C(COOH)CYCCOC + OH	7.93×10^{37}	−8.02	22 442	8.29×10^{-1}	2.25	−8357	0.1
C_3•CCOOH + O_2 → C(COOH)CYCCOC + OH	1.14×10^{3}	3.20	15 575	6.42×10^{3}	1.20	−4803	1
C_3•CCOOH + O_2 → C(COOH)CYCCOC + OH	2.57×10^{-38}	16.09	6352	2.90×10^{16}	−2.24	6831	10
C_3•CCOOH + O_2 → C(COOH)CYCCOC + OH	4.379×10^{-43}	14.36	4040	2.581×10^{-22}	7.23	3140	k_∞[e]
C_3•CCOOH + O_2 → C═C(C)COOH + CH_2O + OH	1.442×10^{18}	−2.59	3520	5.595×10^{22}	−4.12	3800	k_0
C_3•CCOOH + O_2 → C═C(C)COOH + CH_2O + OH	1.68×10^{49}	−11.89	18 353	4.16×10^{-3}	3.17	−11 007	0.0001
C_3•CCOOH + O_2 → C═C(C)COOH + CH_2O + OH	1.48×10^{52}	−12.54	22 443	5.67×10^{-3}	3.13	−10 883	0.01
C_3•CCOOH + O_2 → C═C(C)COOH + CH_2O + OH	6.64×10^{37}	−7.69	21 955	4.11×10^{-2}	2.90	−10 095	0.1
C_3•CCOOH + O_2 → C═C(C)COOH + CH_2O + OH	2.34×10^{3}	3.41	15 193	6.47×10^{2}	1.76	−6244	1
C_3•CCOOH + O_2 → C═C(C)COOH + CH_2O + OH	1.83×10^{-37}	16.13	6136	3.81×10^{15}	−1.71	5547	10
C_3•CCOOH + O_2 → C═C(C)COOH + CH_2O + OH	9.885×10^{-43}	14.53	3580	3.242×10^{-22}	7.47	2560	k_∞[e]
C_2C(COOH)COO• → C_2C(COOH)CHO + OH $_{(TS8)}$	1.213×10^{95}	−25.22	33 370	4.767×10^{26}	−5.21	−5340	k_0[c]
C_2C(COOH)COO• → C_2C(COOH)CHO + OH $_{(TS8)}$	2.88×10^{34}	−8.28	29 474	3.78×10^{11}	−2.28	8392	0.0001
C_2C(COOH)COO• → C_2C(COOH)CHO + OH $_{(TS8)}$	8.26×10^{24}	−5.12	27 111	4.62×10^{26}	−6.28	20 290	0.01
C_2C(COOH)COO• → C_2C(COOH)CHO + OH $_{(TS8)}$	1.08×10^{16}	−2.21	24 815	1.13×10^{41}	−9.92	34 494	0.1
C_2C(COOH)COO• → C_2C(COOH)CHO + OH $_{(TS8)}$	3.39×10^{9}	−0.08	23 088	2.25×10^{19}	−3.55	21 329	1
C_2C(COOH)COO• → C_2C(COOH)CHO + OH $_{(TS8)}$	1.70×10^{6}	0.99	22 196	5.54×10^{26}	−5.38	29 058	10
C_2C(COOH)COO• → C_2C(COOH)CHO + OH $_{(TS8)}$	9.808×10^{5}	1.07	21 990	1.741×10^{4}	1.56	20 830	k_∞
C_2C(COOH)COO• → C_2C(COOH)CHO + OH $_{(TS8A)}$	1.569×10^{61}	−14.69	46 930	6.193×10^{37}	−7.08	42 970	k_0
C_2C(COOH)COO• → C_2C(COOH)CHO + OH $_{(TS8A)}$	7.98×10^{81}	−23.82	56 977	2.08×10^{15}	−4.74	14 556	0.0001
C_2C(COOH)COO• → C_2C(COOH)CHO + OH $_{(TS8A)}$	4.92×10^{68}	−19.01	55 177	1.08×10^{36}	−9.97	30 537	0.01
C_2C(COOH)COO• → C_2C(COOH)CHO + OH $_{(TS8A)}$	4.25×10^{48}	−12.18	50 845	3.28×10^{57}	−15.23	51 214	0.1
C_2C(COOH)COO• → C_2C(COOH)CHO + OH $_{(TS8A)}$	2.41×10^{28}	−5.46	45 861	6.42×10^{26}	−6.03	32 691	1
C_2C(COOH)COO• → C_2C(COOH)CHO + OH $_{(TS8A)}$	2.72×10^{14}	−0.89	42 227	2.51×10^{40}	−9.33	46 453	10
C_2C(COOH)COO• → C_2C(COOH)CHO + OH $_{(TS8A)}$	3.716×10^{8}	1.02	40 510	6.631×10^{6}	1.51	39 340	k_∞

TABLE 8 (Continued)

	$T = 300-900$ K			$T = 900-2500$ K			
	A^b	n	E_a	A	n	E_a	P (atm)
$C_2C(COOH)COO^\bullet \rightarrow C_2C(CH_2O^\bullet)COO^\bullet + OH$	2.239×10^{66}	−15.03	49 260	1.913×10^{46}	−8.42	46 920	k_0 [c]
$C_2C(COOH)COO^\bullet \rightarrow C_2C(CH_2O^\bullet)COO^\bullet + OH$	3.31×10^{94}	−26.81	59 863	5.58×10^{23}	−6.47	15 616	0.0001
$C_2C(COOH)COO^\bullet \rightarrow C_2C(CH_2O^\bullet)COO^\bullet + OH$	9.73×10^{82}	−22.41	58 882	8.27×10^{44}	−11.74	31 841	0.01
$C_2C(COOH)COO^\bullet \rightarrow C_2C(CH_2O^\bullet)COO^\bullet + OH$	4.45×10^{62}	−15.41	54 777	1.68×10^{67}	−17.15	53 210	0.1
$C_2C(COOH)COO^\bullet \rightarrow C_2C(CH_2O^\bullet)COO^\bullet + OH$	3.01×10^{40}	−8.02	49 433	2.67×10^{35}	−7.60	33 996	1
$C_2C(COOH)COO^\bullet \rightarrow C_2C(CH_2O^\bullet)COO^\bullet + OH$	2.35×10^{24}	−2.73	45 271	5.58×10^{49}	−11.06	48 438	10
$C_2C(COOH)COO^\bullet \rightarrow C_2C(CH_2O^\bullet)COO^\bullet + OH$	7.546×10^{16}	−0.29	43 110	1.151×10^{15}	0.22	41 920	k_∞
$C_2C(COOH)COO^\bullet \rightarrow C_2^\bullet C(COOH)_2$	2.844×10^{110}	−27.46	32 620	4.907×10^{123}	−30.92	44 710	k_0 [f]
$C_2C(COOH)COO^\bullet \rightarrow C_2^\bullet C(COOH)_2$	3.06×10^{37}	−8.91	30 537	1.04×10^{13}	−2.44	8576	0.0001
$C_2C(COOH)COO^\bullet \rightarrow C_2^\bullet C(COOH)_2$	3.65×10^{27}	−5.62	28 090	2.49×10^{28}	−6.52	20 699	0.01
$C_2C(COOH)COO^\bullet \rightarrow C_2^\bullet C(COOH)_2$	1.79×10^{18}	−2.56	25 690	1.19×10^{43}	−10.23	35 180	0.1
$C_2C(COOH)COO^\bullet \rightarrow C_2^\bullet C(COOH)_2$	2.43×10^{11}	−0.32	23 869	1.01×10^{21}	−3.74	21 801	1
$C_2C(COOH)COO^\bullet \rightarrow C_2^\bullet C(COOH)_2$	7.36×10^{7}	0.83	22 919	4.28×10^{28}	−5.63	29 765	10
$C_2C(COOH)COO^\bullet \rightarrow C_2^\bullet C(COOH)_2$	2.381×10^{7}	0.98	22 630	4.383×10^{5}	1.47	21 470	k_∞
$C_2^\bullet C(COOH)_2 \rightarrow C(COOH)CYCCOC + OH$	1.139×10^{21}	−1.87	13 260	1.704×10^{25}	−3.21	13 940	k_0
$C_2^\bullet C(COOH)_2 \rightarrow C(COOH)CYCCOC + OH$	3.50×10^{52}	−14.86	24 220	5.37×10^{18}	−4.44	9892	0.0001
$C_2^\bullet C(COOH)_2 \rightarrow C(COOH)CYCCOC + OH$	2.80×10^{35}	−8.71	21 325	4.66×10^{31}	−7.70	16 450	0.01
$C_2^\bullet C(COOH)_2 \rightarrow C(COOH)CYCCOC + OH$	3.29×10^{34}	−7.88	22 946	1.55×10^{14}	−2.18	8606	0.1
$C_2^\bullet C(COOH)_2 \rightarrow C(COOH)CYCCOC + OH$	5.94×10^{22}	−3.90	20 341	1.41×10^{19}	−3.21	13 887	1
$C_2^\bullet C(COOH)_2 \rightarrow C(COOH)CYCCOC + OH$	2.70×10^{12}	−0.52	17 633	1.42×10^{45}	−10.00	36 847	10
$C_2^\bullet C(COOH)_2 \rightarrow C(COOH)CYCCOC + OH$	7.802×10^{4}	1.78	14 630	1.998×10^{6}	1.34	15 070	k_∞
$C_2^\bullet C(COOH)_2 \rightarrow C{=}C(C)COOH{+}CH_2O + OH$	1.154×10^{20}	−1.32	11 640	1.170×10^{25}	−2.91	12 660	k_0 [c]
$C_2^\bullet C(COOH)_2 \rightarrow C{=}C(C)COOH{+}CH_2O + OH$	2.67×10^{52}	−14.39	23 988	3.09×10^{18}	−3.93	9640	0.0001
$C_2^\bullet C(COOH)_2 \rightarrow C{=}C(C)COOH{+}CH_2O + OH$	1.69×10^{36}	−8.59	21 153	3.65×10^{29}	−6.70	15 184	0.01
$C_2^\bullet C(COOH)_2 \rightarrow C{=}C(C)COOH{+}CH_2O + OH$	1.47×10^{35}	−7.76	22 566	2.92×10^{13}	−1.62	7988	0.1
$C_2^\bullet C(COOH)_2 \rightarrow C{=}C(C)COOH{+}CH_2O + OH$	2.69×10^{24}	−4.13	20 174	1.50×10^{18}	−2.61	12 980	1
$C_2^\bullet C(COOH)_2 \rightarrow C{=}C(C)COOH{+}CH_2O + OH$	1.11×10^{15}	−1.06	17 714	3.55×10^{42}	−8.98	34 495	10
$C_2^\bullet C(COOH)_2 \rightarrow C{=}C(C)COOH{+}CH_2O + OH$	5.828×10^{4}	2.07	13 600	1.463×10^{6}	1.63	14 040	k_∞

[a] Geometric mean frequency from CPFIT. $C_2C(COOH)COO^\bullet$: 411.6 cm^{-1} (22.044), 1426.9 cm^{-1} (21.563), 3924.1 cm^{-1} (6.893), $C_2^\bullet C(COOH)_2$: 390.5 cm^{-1} (22.354), 1426.8 cm^{-1} (21.032), 3906.2 cm^{-1} (6.614). Lennard-Jones parameters: $\sigma = 6.40$ Å, $\epsilon/k = 720.5$ K. [b] Units for A in s^{-1} or $cm^3\ mol^{-1}\ s^{-1}$ and units for E_a in cal mol^{-1}. [c] Low-pressure limit: multiply rate by [M]. [d] High-pressure limit: multiply rate by $[M]^{-1}$. [e] High-pressure limit: multiply rate by $[M]^{-2}$. [f] Low-pressure limit: multiply rate by $[M]^2$.

pressure-limit rate constants show good agreement with the experimentally determined rate constant reported by Slagle et al.[61]

The unimolecular decomposition of the neopentyl radical to isobutene + CH_3 is important to the OH radical decay, as shown in the following OH sensitivity analysis. The OH radical generated by the neopentyl oxidation reactions and the methyl radical from the β-scission reaction above will add to isobutene forming new isobutene adducts: $C_3^\bullet COH$, $C_2C^\bullet COH$, and $C_2C^\bullet CC$. These OH and CH_3 addition reactions and the subsequent O_2 association reactions with these adducts have been calculated by ab initio and DFT methods and included in our mechanism, but these reactions show little contribution to the OH formation profile; isobutene oxidation reactions[62] are important only for modeling the primary initial product isobutene-formation profile.

5. Model and Comparison with Experimental Results. A detailed reaction mechanism (322 reactions, 138 species) for the neopentyl radical oxidation is assembled in Supporting Information Table S4, where the CHEMKIN II interpreter and integrator (version 3.1)[59] are used to model the experimental OH-formation profile for the reaction time of 0−3 ms. Abstraction reactions are not considered to be pressure-dependent and therefore do not require falloff analysis. Abstraction reactions of O, OH, HO_2, and $R^\bullet$ radicals are taken from evaluated literature wherever possible. A procedure from Dean and Bozzelli[63] is used to estimate abstraction rate constants by H, O, OH, and CH_3 radicals when no literature data are available.

The time dependence of the OH radical formation profile predicted by our reaction mechanism and compared with experimental data published by Hughes et al.[9] is shown in Figure 12. The experiment was performed at 700 K and 613.3 Torr, with an O_2 pressure of 63.3 Torr and a $C_3CC^\bullet$ radical concentration of 3×10^{11} molecule cm^{-3}. The solid curve in Figure 12 represents our modeling result for the OH profile,

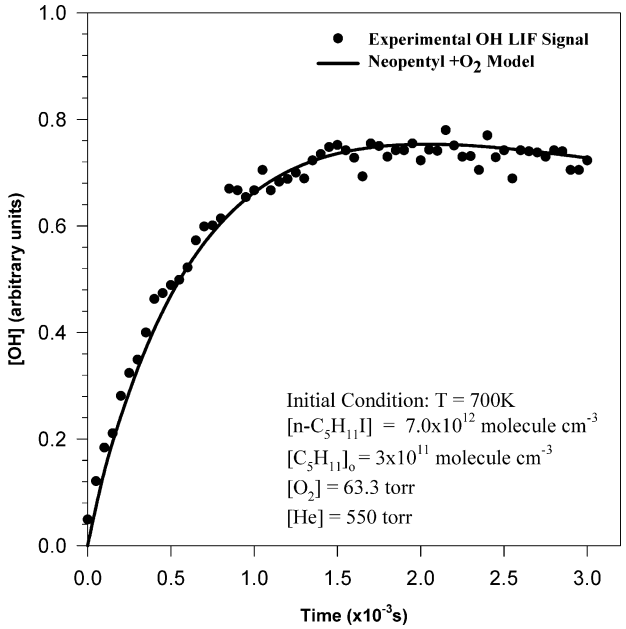

Figure 12. Comparison of the present model with the experimental OH LIF measurements of Hughes et al.[9]

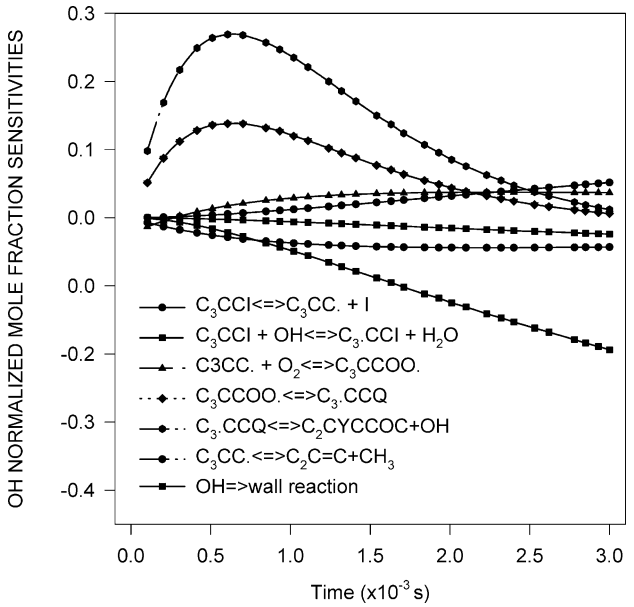

Figure 13. Sensitivity analysis of OH formation at $T = 700$ K and $P = 613.3$ Torr.

and it shows good agreement with the experimental data of Hughes et al.[9] Sensitivity analysis of OH formation at the experimental temperature and pressure is shown in Figure 13. The reaction channel for the formation of 3,3-dimethyloxetane + OH is calculated to have the highest sensitivity for the formation of the OH radical and the isomerization to C_3•CCOOH from the C_3CCOO• radical is next; the well depth of the chemical activation reaction of C_3CC• + O_2 for the formation of neopentyl peroxy and the unimolecular decomposition of the neopentyliodide radical are also important.

The decay of the OH radical is the most sensitive to the OH wall reaction, and this rate constant is taken to be 88 s^{-1} as measured in the flow system by Hughes et al.[9] The reaction of OH with $C_5H_{11}I$ is also sensitive, as confirmed by independent experiments in which OH was generated at 193 nm from N_2O/H_2O/He mixtures.[9] The unimolecular decomposition of the neopentyl radical to isobutene + CH_3 is shown to be important to the OH decay because it results in the loss of the OH precursor.

Overall, there are a number of reaction sets responsible for the OH formation: (i) the chemical activation reaction of the neopentyl radical + O_2 with isomerization and subsequent dissociation reactions; (ii) the addition of a second O_2 to the hydroperoxy-neopentyl radical with isomerization and subsequent dissociation reactions; (iii) the addition and subsequent oxidation reactions of isobutene from neopentyl and hydroperoxy-neopentyl radical dissociation, and (iv) the oxidation of the initial products and intermediates generated in the neopentyl oxidation system. The importance of these reaction paths changes with concentrations, pressure, and temperature. At a pressure of 613.3 Torr and a temperature of 700 K, the formation of 3,3-dimethyloxetane + OH is the most important channel to form the OH radical.

Walker et al.[13] measured the absolute concentration of a number of stable hydrocarbon and oxyhydrocarbon products as a function of neopentane oxidation (conversion) in an oxidizing environment using a flow reactor. Their experiment was carried out at 753 K and 500 Torr total pressure for three mixtures containing 5 Torr of neopentane in bath gases of nitrogen, oxygen, and hydrogen. We calculate the absolute concentrations of initial primary products 3,3-dimethyloxetane and isobutene

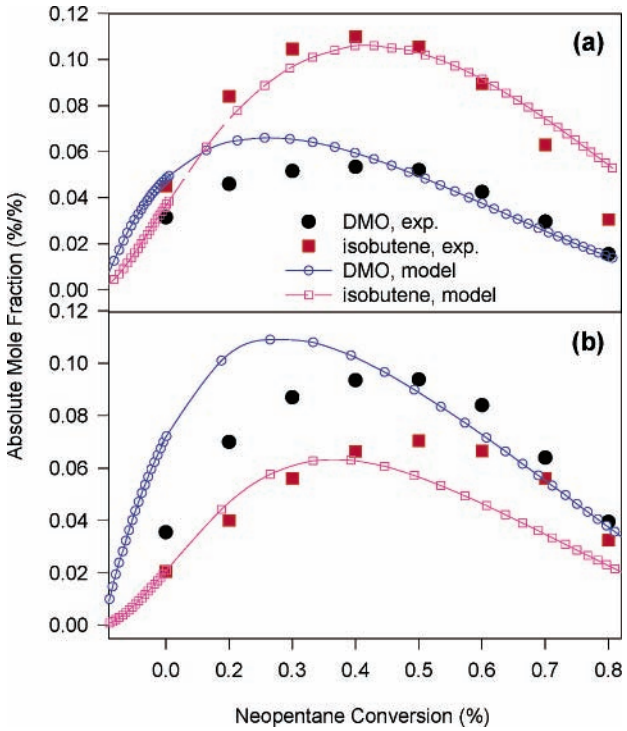

Figure 14. Comparison of the present model with the experimental measurements of initial primary products by Walker et al.[13] at $T = 753$ K and $P = 500$ Torr containing 5 Torr of neopentane. (a) $H_2 = 425$, $O_2 = 70$ Torr; (b) $H_2 = 140$, $O_2 = 355$ Torr. DMO stands for 3,3-dimethyloxetane.

with our kinetic mechanism, along with the appropriate QRRK/master equation analysis at these temperature, bath gas, and pressure conditions. Initial product yields are compared with the experimental results of Walker et al.[13] in Figure 14; these results are from the use of our calculated kinetic parameters at a pressure of 500 Torr with a specific bath gas. We note that our current mechanism predicts initial reaction products for the neopentyl + O_2 reaction system; specifically, it does not include all the secondary reactions of most initial products. The concentrations of 3,3-dimethyloxetene and isobutene predicted theoretically show overall agreement with the experimental measurements for two mixtures at very different oxygen concentrations: (a) hydrogen-rich: $H_2 = 425$, $O_2 = 70$ Torr; (b) oxygen-rich: $H_2 = 140$, $O_2 = 355$ Torr. We note that the differences in the experiment versus model may arise from our mechanism being somewhat incomplete, and we are working on secondary and final reactions for this system for further publication. We do not have paths for most of the initial reaction products to intermediates and final CO_2 and H_2O species in this present study.

Summary

Thermochemical properties of the neopentyl radical + oxygen reaction system and the hydroperoxy neopentyl radical + O_2 reaction system are calculated using ab initio CBS-Q and density functional B3LYP/6-311++G(3df,2p) methods. The barriers for the isomerization of neopentyl peroxy and subsequent epoxide formation reactions are calculated to be 23.82 and 15.50 kcal mol^{-1}, respectively. Kinetic parameters for intermediate and product-formation channels are calculated versus temperature and pressure. A mechanism describing reaction paths and kinetic parameters for the initial steps in the neopentyl oxidation reaction system is developed to model the experimental OH-formation profile. Second O_2 addition to the hydroperoxy

neopentyl radical has a minor contribution to the OH profile under the modeled conditions but can be important to chain branching. Several reactions are predicted to be important to the OH-formation profile. Thermodynamic equilibria for the reactions of $C_3CCOO^{\bullet} \leftrightarrow C_3^{\bullet}CCOOH$ and reactions $C_3^{\bullet}C$-COOH → 3,3-dimethyloxetane + OH and $C_2C{=}C + CH_2O +$ OH serve to control the oxidation rate in this 700 K, 613.3 Torr reaction system. The concentrations of two observed, initial products in this system, 3,3-dimethyloxetane and isobutene, are also calculated by the model and compared with the experimental results.

Acknowledgment. This research is supported by the USEPA Northeast Regional Research Center and the USEPA Airborne Organics Research Center. We acknowledge Dr. Graig A. Taatjes from Sandia National Laboratories for providing experimental data for HO_2 formation and preprints to publication. We also thank Dr. Chiung-Chu Chen for helpful discussions and Leonhard Rutz for help in compiling and maintaining computer programs and systems.

Supporting Information Available: Optimized structural parameters of 33 species, including transition-states structures, the corresponding unscaled vibrational frequencies, and moments of inertia. Thermodynamic analyses for reactions of neopentyl radical oxidation. A detailed reaction mechanism for the neopentyl radical oxidation used to model the OH-formation profile. Pressure-dependent rate constants of $C_3CCOO^{\bullet} + O_2$ and $C_3^{\bullet}CCOOH + O_2$ reaction systems in Chebyshev polynominal format. This material is available free of charge via the Internet at http://pubs.acs.org.

References and Notes

(1) Bozzelli, J. W.; Dean, A. M. *J. Phys. Chem.* **1990**, *94*, 3313.
(2) Bozzelli, J. W.; Pitz, W. J. *Symp. Int. Combust. Proc.* **1994**, *25*, 783.
(3) Norton, T. S.; Dryer, F. L. *Int. J. Chem. Kinet.* **1992**, *24*, 319.
(4) Warnatz, J. *Proc. Combust. Inst.* **1985**, *20*, 845.
(5) Chen, C.-J.; Bozzelli, J. W. *J. Phys. Chem. A* **1999**, *103*, 9731.
(6) Sheng, C. Y.; Bozzelli, J. W.; Dean, A. M.; Chang, A. Y. *J. Phys. Chem. A* **2002**, *106*, 7276.
(7) DeSain, J. D.; Klippenstein, S. J.; Taatjes, C. A. *Phys. Chem. Chem. Phys.* **2003**, *5*, 1584.
(8) Hughes, K. J.; Lightfoot, P. D.; Pilling, M. J. *Chem. Phys. Lett.* **1992**, *191*, 581.
(9) Hughes, K. J.; Halford-Maw, P. A.; Lightfood, P. D.; Turanyi, T.; Pilling, M. J. *Symp. Int. Combust. Proc.* **1992**, *24*, 645.
(10) Baldwin, R. R.; Hisham, M. W. M.; Walker, R. W. *J. Chem. Soc., Faraday Trans.* **1982**, *78*, 1615.
(11) Wu, D.; Bayes, K. D. *Int. J. Chem. Kinet.* **1986**, *18*, 547.
(12) Xi, Z.; Han, W. J.; Bayes, K. D. *J. Phys. Chem.* **1988**, *92*, 3450.
(13) Baker, R. R.; Baldwin, R. R.; Everett, C. J.; Walker, R. W. *Combust. Flame* **1975**, *25*, 285.
(14) Baker, R. R.; Baldwin, R. R.; Walker, R. W. *Combust. Flame* **1976**, *27*, 147.
(15) Dagaut, P.; Cathonnet, M. *Combust. Flame* **1999**, *118*, 191.
(16) Tsuzuki, S.; Uchimaru, T.; Tanabe, K.; Hirano, T. *J. Phys. Chem.* **1993**, *97*, 1346.
(17) Wang, S. M.; David, L.; Cernansky, N. P.; Curran, H. J.; Pitz, W. J.; Westbrook, C. K. *Combust. Flame* **1999**, *118*, 415.
(18) Curran, H. J.; Pitz, W. J.; Westbrook, C. K.; Hisham, M. W. M.; Walker, R. W. *Symp. Int. Combust. Proc.* **1996**, *26*, 641.
(19) Ritter, E. R.; Bozzelli, J. W. *Int. J. Chem. Kinet.* **1991**, *23*, 767.
(20) Westmoreland, P. R. *Combust. Sci. Technol.* **1992**, *82*, 151.
(21) Dean, A. M.; Westmoreland, P. R. *Int. J. Chem. Kinet.* **1987**, *19*, 207.
(22) Bozzelli, J. W.; Dean, A. M. *J. Phys. Chem.* **1993**, *97*, 4427.
(23) Chang, A. Y.; Bozzelli, J. W.; Dean, A. M. *Z. Phys. Chem. (Muenchen)* **2000**, *214*, 1533.
(24) Stewart, J. J. P. *MOPAC 6.0*; Frank J. Seiler Research Lab, U. S. Air Force Academy: Colorado, 1990.
(25) Frisch, M. J.; Trucks, G. W.; Schlegel, H. B.; Scuseria, G. E.; Robb, M. A.; Cheeseman, J. R.; Zakrzewski, V. G.; Montgomery, J. A., Jr.; Stratmann, R. E.; Burant, J. C.; Dapprich, S.; Millam, J. M.; Daniels, A. D.; Kudin, K. N.; Strain, M. C.; Farkas, O.; Tomasi, J.; Barone, V.; Cossi, M.; Cammi, R.; Mennucci, B.; Pomelli, C.; Adamo, C.; Clifford, S.; Ochterski, J.; Petersson, G. A.; Ayala, P. Y.; Cui, Q.; Morokuma, K.; Malick, D. K.; Rabuck, A. D.; Raghavachari, K.; Foresman, J. B.; Cioslowski, J.; Ortiz, J. V.; Stefanov, B. B.; Liu, G.; Liashenko, A.; Piskorz, P.; Komaromi, I.; Gomperts, R.; Martin, R. L.; Fox, D. J.; Keith, T.; Al-Laham, M. A.; Peng, C. Y.; Nanayakkara, A.; Gonzalez, C.; Challacombe, M.; Gill, P. M. W.; Johnson, B. G.; Chen, W.; Wong, M. W.; Andres, J. L.; Head-Gordon, M.; Replogle, E. S.; Pople, J. A. *Gaussian 98*, revision A.9; Gaussian, Inc.: Pittsburgh, PA, 1998.
(26) McGrath, M. P.; Radom, L. *J. Chem. Phys.* **1991**, *94*, 511.
(27) Glukhovtsev, M. N.; Pross, A.; McGrath, M. P.; Radom, L. *J. Chem. Phys.* **1995**, *103*, 1878.
(28) *GaussView*, 2.1 ed.; Gaussian, Inc.: Pittsburgh, PA, 1998.
(29) Lay, T. H.; Bozzelli, J. W.; Dean, A. M.; Ritter, E. R. *J. Phys. Chem.* **1995**, *99*, 14514.
(30) Gilbert, R. G.; Luther, K.; Troe, J. *Ber. Bunsen-Ges. Phys. Chem.* **1983**, *87*, 169.
(31) Dean, A. M.; Bozzelli, J. W.; Ritter, E. R. *Combust. Sci. Technol.* **1991**, *80*, 63.
(32) Ben-Amotz, D.; Herschbach, D. R. *J. Phys. Chem.* **1990**, *94*, 1038.
(33) Good, W. D. *J. Chem. Thermodyn.* **1970**, *2*, 237.
(34) Sumathi, R.; Carstensen, H.-H.; Green, W. H., Jr. *J. Phys. Chem. A* **2001**, *105*, 6910.
(35) Holmes, J. L.; Lossing, F. P.; Maccoll, A. *J. Am. Chem. Soc.* **1988**, *110*, 7339.
(36) Knyazev, V. D.; Slagle, I. R. *J. Phys. Chem.* **1998**, *102*, 1770.
(37) Clifford, E. P.; Wenthold, P. G.; Gareyev, R.; Lingberger, W. C.; Depuy, C. H.; Bierbaum, V. M.; Ellison, G. B. *J. Chem. Phys* **1998**, *109*, 10293.
(38) Chen, C.-J.; Bozzelli, J. W. *J. Phys. Chem. A* **2000**, *104*, 4997.
(39) Ervin, K. M. G.; Scott; Barlow, S. E.; Gilles, M. K.; Harrison, A. G.; Bierbaum, V. M.; DePuy, C. H.; Lineberger, W. C.; Ellison, G. B. *J. Am. Chem. Soc.* **1990**, *112*, 5750.
(40) Blanksby, S. J.; Ramond, T. M.; Davico, G. E.; Nimlos, M. R.; Kato, S.; Bierbaum, V. M.; Lineberger, W. C.; Ellison, G. B.; Okumura, M. *J. Am. Chem. Soc.* **2001**, *123*, 9585.
(41) Holmes, J. L.; Lossing, F. P.; Mayer, P. M. *J. Am. Chem. Soc.* **1991**, *113*, 9723.
(42) Curtiss, L. A.; Lucas, D. J.; Pople, J. A. *J. Chem. Phys.* **1995**, *102*, 3292.
(43) *Heats of Formation of Organic Free Radicals by Kinetic Methods in Energetics of Organic Free Radicals*; Tsang, W., Martinho Simoes, J. A., Greenberg, A., Liebman, J. F., Eds.; Blackie Academic and Professional: London, 1996.
(44) Frenkel, M.; Kabo, G. J.; Marsh, K. N. *Thermodynamics of Organic Compounds in the Gas State*; Thermodynamic Research Center, Texas A&M University: College Station, TX, 1994.
(45) Ruscic, B.; Berkowitz, J. *J. Phys. Chem.* **1993**, *97*, 11451.
(46) Dobe, S. B. T.; Turanyi, T. M. F.; Grussdorf, J.; Temps, F.; Wagner, H. G. *J. Phys. Chem.* **1996**, *100*, 19864.
(47) Ramond, T. M.; Davico, G. E.; Schwartz, R. L.; Lineberger, W. C. *J. Chem. Phys.* **2000**, *112*, 1158.
(48) Sun, H.; Chen, C.-J.; Bozzelli, J. W. *J. Phys. Chem. A* **2000**, *104*, 8270.
(49) Sun, H.; Bozzelli, J. W. *J. Phys. Chem. A* **2003**, *107*, 1018.
(50) Wijaya, C. D.; Sumathi, R.; Green, W. H., Jr. *J. Phys. Chem. A* **2003**, *107*, 4908.
(51) We cannot find this transition-state structure, and this reaction is 20.6 kcal/mol exothermic.
(52) Chen, C.-J.; Bozzelli, J. W. *J. Phys. Chem. A* **2000**, *104*, 9715.
(53) Sheng, C. Representative Hydrocarbon Oxidation Model and Detailed Mechanism for Combustion of a Complex Solid Fuel in a Pilot Scale Incinerator. Ph.D. Dissertation, New Jersey Institute of Technology, Newark, NJ, 2002.
(54) Venkatesh, P. K.; Dean, A. M.; Cohen, M. H.; Carr, R. W. *Rev. Chem. Eng.* **1997**, *13*, 67.
(55) Stewart, P. H.; Larson, C. W.; Golden, D. *Combust. Flame* **1989**, *75*, 25.
(56) Poole, J. S.; Gilbert, R. G. *Int. J. Chem. Kinet.* **1994**, *26*, 273.
(57) Venkatesh, P. K.; Chang, A. Y.; Dean, A. M.; Cohen, M. H.; Carr, R. W. *AIChE J.* **1997**, *43*, 1331.
(58) Tsang, W. *Chemical and Physical Process in Combustion*; The 2003 Technical Meeting of the Eastern States Section of the Combustion Institute, 2003.
(59) Kee, R. J.; Rupley, F. M.; Miller, J. A. *Chemkin-II: A Fortran Chemical Kinetics Package for Analysis of Gas-Phase Chemical Kinetics*, version 3.1; Sandia National Laboratories, Combustion Research Facility: Livermore, CA, 1990.
(60) Kee, R. J.; Rupley, F. M.; Meeks, E.; Miller, J. A. *Chemkin-III: A Fortran Chemical Kinetics Package for Analysis of Gas-Phase Chemical Kinetics*, version 3.6.2; Reaction Design, Inc: San Diego, CA, 2001.

(61) Slagle, I. R.; Batt, L.; Gmurczyk, G. W.; Gutman, D.; Tsang, W. *J. Phys. Chem.* **1991**, *95*, 7732.
(62) Chen, C.-J. B.; Joseph, W. *J. Phys. Chem. A* **2000**, *104*, 9715.
(63) Dean, A. M.; Bozzelli, J. W. Combustion Chemistry of Nitrogen. In *Gas-Phase Combustion Chemistry*;Gardiner, W. C., Ed.; Springer-Verlag: New York, 2000.